Structural and Energetic Characterization of the Major DNA Adduct Formed from the Food Mutagen Ochratoxin A in the *Nar*I Hotspot Sequence: Influence of Adduct Ionization on the Conformational Preferences and Implications for the NER Propensity

Purshotam Sharma[1], Richard A. Manderville[2] and Stacey D. Wetmore[1,*]

[1]Department of Chemistry and Biochemistry, University of Lethbridge, Lethbridge, Alberta, Canada, T1K 3M4 and [2]Department of Chemistry and Toxicology, University of Guelph, Guelph, Ontario, Canada, N1G 2W1

[*]To whom correspondence should be addressed. Tel. +1 403 329-2323; Fax: +1 403 329-2057; Email: stacey.wetmore@uleth.ca

SUPPLEMENTARY MATERIALS AND METHODS

Starting Structures. Molecular dynamics (MD) simulations were carried out with the neutral, monoanionic or dianionic form of the OTB-dG adduct at the G^1, G^2 or G^3 position in the *Nar*I sequence and paired against complementary cytosine. Initial structures for three (major groove, (minor groove) wedge and base-displaced intercalated (stacked)) conformations were built from the natural *Nar*I DNA helix using the NAB module of AMBER 11 [1] and adding the C8-moiety to the guanine residue under consideration using GaussView (Version 5). The starting adduct orientation for the major-groove conformation was built by placing the adduct in the *anti* conformation, and allowing the lesion to form Watson-Crick hydrogen bonds with the opposing C. On the other hand, the wedge conformation was built by orienting the adduct in the *syn* conformation and permitting Hoogsteen hydrogen bonding with C. The starting structure for the base-displaced intercalated (stacked) conformation was built by displacing the opposing cytosine out of the helix and using the *syn* orientation of the adduct, while allowing intercalation of the C8-moiety. Two OTA rotamers (α and β, Figure S1) were considered that are defined along the axis passing through the two fused rings of the OTA isocoumarin moiety, are governed by the dihedral angle θ, and are related by an approximate 180° flip along the θ torsion angle (∠(N9C8C1C2), Figure 1). Both rotamers were used to model each conformation. In addition, simulations were carried out using a number of different trial structures corresponding to the α and β rotamers for the *syn* (wedge and base-displaced intercalated) conformations in order to search for the lowest energy structures that retain optimal characteristics of the base-displaced intercalated and wedge conformations. Since our main goal is to understand the conformational preferences of OTB-dG at each of the G^1, G^2 and G^3 positions, an additional filter that retains Watson-Crick hydrogen bonding at the terminal base pairs of the 12-mer helix was applied to ensure the viability of the simulated structures for the free energy calculations. This technicality was necessary since destabilizing perturbations at the ends of the helix may alter the overall free energy of the simulated

helix, which makes it difficult to isolate the effect of the adduct conformation on the helix stability. The retention of the terminal base pairs was confirmed by monitoring the corresponding Watson-Crick hydrogen bonds (Table S7).

Force Field. The parameters for the bonded terms in the force field for simulating the natural nucleotides were taken from the parmbsc0 modification to the parm99 force field, and additional parameters for the modified residues were assigned based on the generalized AMBER force field (GAFF) [2]. The RED.v.III.4 [3] program was used to calculate the partial charges for building the force field libraries of ionized OTA, while the partial charges for neutral OTA were taken from a previous study [4]. A two-stage RESP fitting procedure was carried out on B3LYP/6-31G(d) optimized structures using Hartee-Fock single-point calculation with the 6-31G(d) basis set and the Gaussian 03-interfaced RED program. Antechamber 1.4 [5] was then used to assign atom types. The partial charges and atom types for the modified residues are given in Tables S8-S10.

MD Protocol. Simulations were carried out using PMEMD of the AMBER 11 [1] or 12 [6] software package. Each simulated DNA duplex was first neutralized with 22 sodium ions and solvated in an 8 Å truncated octahedral TIP3P [7] box of water molecules using the LEAP module of AMBER 11[1]. The particle mesh Ewald (PME) method was used to model the long-range Coulombic interactions, and a 10 Å cutoff was applied to the Lennard-Jones interactions. The bonds involving hydrogen atoms were constrained using the SHAKE algorithm. A 2 fs time step was used. Initial minimization was carried out using 500 steps of steepest descent (SD) and 500 steps of conjugate gradient (CG) optimization, where the solute was held fixed using a force constant of 500 kcal mol^{-1} $Å^{-2}$. The entire system was then relaxed using 1000 and 1500 steps of SD and CG minimization, respectively. Next, the system was heated from 0 to 300 K using the Langevin thermostat for 20 ps under constant volume conditions. Finally, unrestrained production simulations were carried out at constant temperature (300 K) and pressure (1 atm) for 40 nanoseconds (ns).

Free Energy Analysis. Free energy analysis was carried out on snapshots from MD trajectories with the water and counterions removed using the MM-PBSA [8] method as implemented in AMBER 11 [1] or 12 [6]. A total of 1000 snapshots at 20 ps intervals were used to calculate the binding free energy (E_{MM}) and the implicit solvation free energy (E_{sol}) terms, while 100 snapshots at 200 ps intervals were used across the entire 40 ns trajectory to calculate the vibrational entropy contributions using the normal-mode analysis.

The total free energy (G_{Tot}) was calculated as

$$G_{Tot} = E_{MM} + E_{sol} - TS$$

Within this formulism, the E_{MM} term was calculated as the sum of an internal energy term (E_{int}), which consists of deviations in bonds (E_{bonds}), angles (E_{angles}) and dihedral angles ($E_{dihedrals}$) from their equilibrium values, the van der Waals interaction energies (E_{vdW}) and the electrostatic energies (E_{elec}).

$$E_{MM} = E_{int} + E_{vdW} + E_{elec}$$

$$E_{int} = E_{bonds} + E_{angles} + E_{dihedrals}$$

The E_{sol} term was calculated as the sum of the polar and nonpolar contributions. The polar contribution stemming from the electrostatic solvation free energies was calculated using the Poisson Boltzmann (PB) model. The nonpolar contributions were calculated based on the solvent accessible surface area, which was evaluated using Sanner's algorithm.

RMSD. The root mean square deviation (RMSD) of the atoms forming the sugar–phosphate backbone was used to evaluate the stabilities of each simulation. The RMSD of each snapshot in the trajectory was evaluated relative to the first frame, and plotted as a function of time (Figures S7-S9). The mean and standard deviations in the RMSD are given in Table S11, where the fluctuations around the mean range from 0.348 to 0.787 Å. Thus, the entire 40 ns structural ensemble was used for the free energy calculations and further structural analyses.

Representative Structures. Representative structures were obtained by clustering each MD simulation with respect to the χ and θ dihedral angles of the OTB-dG residue using the refinement (K-means) clustering algorithm as implemented in the cpptraj module of Ambertools. The means clustering algorithm choses a collection of maximally distant seed points, each of which are assigned to a cluster. This procedure is then iterated over all data points. Each data point is then assigned to the cluster with the closest centroid. The centroid of the cluster is then recomputed, which assigns the frames from the trajectory into a cluster, and identifies the representative structure. All representative structures are provided in Figures S1–S6.

Hydrogen-Bond Occupancies. The hydrogen-bond occupancies were calculated for the trimeric portion of each simulated helix, which includes the adducted base pair and the corresponding 3′- and 5′-neighboring pairs, using the ptraj module of Ambertools. The occupancies were calculated using a donor–acceptor cutoff distance of 3.40 Å and a donor–hydrogen acceptor cutoff angle of 120°. All hydrogen bonds in the trimeric portions, along with their occupancies, are listed in Tables S4–S6. The corresponding occupancies for the unmodified control sequence at the analogous positions are provided for comparison. The hydrogen-bond occupancies for other interactions, such as those between terminal pairs or between the adducted pair and the flanking residues, were also calculated using the same donor–acceptor and angle cutoffs.

Dihedral Angle Calculation. The χ and θ dihedral angles in the OTB-dG adduct were calculated using the 'dihedral' command internally stored in the ptraj module of Ambertools. The probability distribution of χ and θ over the simulation was calculated, and the associated radar plots generated using Microsoft Excel (Figures S10–S12). In the radar plots, the values of the torsion angles are plotted on the circumference, with the probability plotted on the radius of the circle.

Sugar Pucker Analysis. The pseudorotational phase angle for the 2′-deoxyribose sugar of the OTB-dG nucleotide was calculated using the 'pucker' command of the cpptraj module of

Ambertools. The pseudorotational angle of the corresponding nucleotide in the natural *Nar*I sequence was also determined using the same procedure. The radar plots for the probability distribution of the sugar pucker were generated using Microsoft Excel (Figures S13–S16).

Hydrogen-bonding Interaction Energies. The hydrogen-bonding interaction energies between the OTB-dG adduct and the opposing cytosine in the major groove and the wedge DNA conformations were calculated using the 'lie' command of cpptraj. For these calculations, the sugar atoms were excluded, and only the electrostatic energies were used to estimate the hydrogen-bonding strengths since the Lennard-Jones nonbonded interaction energies were small for these subsystems (Tables S1-S3).

Stacking interaction energies. For the major groove and wedge conformations, the stacking energies between the adducted base pair and the flanking base pairs were estimated from the Lennard-Jones energies calculated using the lie command of ptraj. However, for the base-displaced intercalated conformations, only the adducted nucleobase moiety was used for the stacking calculations since the opposing cytosine was displaced out of the helix. The sugar atoms were excluded when calculating the stacking energies (Tables S1-S3).

Base step parameters. The base step parameters were calculated using a pseudostep consisting of the base pairs adjacent and 5′ or 3′ with respect to the lesion. These parameters were compared with the corresponding natural parameters to understand the effect of the damage on the structural properties of DNA. The base step parameters were calculated using the 'nastruct' command of cpptraj. The mean values of the base step parameters from each of the 80000 frames of the 40 ns simulation trajectory were used to estimate the difference between these structural parameters in the modified and natural helices (Tables S1-S3).

Minor groove width. The minor groove widths of the DNA duplexes at the lesion site were calculated using cpptraj. The corresponding values were also determined for the unmodified control sequences. The pairs of phosphate atoms used to calculate the minor groove widths at the lesion site for the natural and modified duplexes are given in the footnotes of Tables S1-S3.

Table S1. Salient structural and energetic features of the major groove conformations of OTB-dG adducted DNA in the neutral, monoanionic or dianionic OTA ionization state at the G^1, G^2 or G^3 position in the *Nar*I recognition sequence.

position	OTB-dG form	rotamer	ΔE_{Hbond} (kcal mol^{-1})[a,b]	ΔE_{vdW} (kcal mol^{-1})[a,c]	shift (Å)[a,d]	slide (Å)[a,d]	rise (Å)[a,d]	tilt (deg.)[a,d]	roll (deg.)[a,d]	twist (deg.)[c,d]	minor groove width (Å)[a,e]
G^1	control	–	–29.0	–30.2	0.1	–0.9	6.6	0.2	11.2	60.7	8.0
	neutral	α	–27.1	–33.4	0.1	–1.6	6.3	4.5	7.7	53.3	8.1
		β	–27.5	–34.8	–0.1	–3.0	7.0	3.0	4.9	57.1	6.3
	monoanionic	α	–25.4	–33.1	0.2	–1.7	6.3	4.5	7.9	50.7	8.2
		β	–26.4	–34.1	0.0	–1.8	6.6	1.1	8.1	54.5	7.4
	dianionic	α	–23.2	–33.2	0.2	–1.4	6.3	4.5	10.0	51.9	8.7
		β	–23.9	–30.8	0.2	–1.9	6.5	1.5	10.3	51.5	8.1
G^2	control	–	–28.6	–30.9	0.0	–1.2	6.8	0.5	5.0	68.4	7.4
	neutral	α	–27.2	–34.8	0.1	–2.4	6.8	3.7	2.5	63.3	6.9
		β	–28.3	–36.0	0.0	–2.8	6.9	3.7	4.2	62.7	6.7
	monoanionic	α	–25.0	–33.4	0.6	–2.6	6.8	3.2	4.5	59.5	7.3
		β	–26.6	–35.3	0.1	–2.6	6.9	2.7	3.2	63.8	6.3
	dianionic	α	–22.6	–32.7	0.8	–2.1	6.7	3.7	5.8	57.2	7.6
		β	–24.2	–35.1	0.2	–2.8	6.9	2.4	4.3	62.0	6.7

G^3	control	–	–28.8	–30.7	0.3	–1.0	6.5	2.0	9.8	64.0	7.8
	neutral	α	–27.2	–34.1	0.0	–2.5	6.8	3.8	2.4	62.6	6.3
		β	–28.0	–34.6	0.0	–2.9	7.1	3.4	2.7	62.6	5.6
	monoanionic	α	–25.1	–33.1	0.3	–1.9	6.5	4.9	1.3	60.2	7.0
		β	–26.5	–34.7	0.1	–2.8	7.1	2.8	3.2	62.4	5.6
	dianionic	α	–22.8	–33.0	0.2	–1.5	6.3	5.4	2.6	56.8	7.7
		β	–24.1	–34.3	–0.1	–3.2	7.1	2.3	1.9	58.7	6.3

[a]Average value calculated from 80000 frames, with each frame recorded every 0.5 ps over the entire 40 ns MD trajectory. [b]Electrostatic interaction energy between the nucleobases forming the Watson-Crick base pair at the lesion site. [c]van der Waals interaction energy between the base pair at the lesion site and the flanking base pairs. [d]Calculated by defining a pseudostep consisting of the two base pairs on the 5′- and 3′-side of the adducted pair. [e]Calculated as the distance between the phosphate atom in the 6^{th} and 23^{rd} residues when the adduct is at G^1, the 7^{th} and 22^{nd} residues when the adduct is at G^2, and the 9^{th} residue and the 20^{th} residue when the adduct is at G^3. The residue numbering within the duplex start from the 5′-end of the adducted strand, and runs from the 3′- to 5′-end of the opposing strand (Figure 1).

Table S2. Salient structural and energetic features of the wedge conformations of OTB-dG adducted DNA in the neutral, monoanionic or dianionic OTA ionization state at the G^1, G^2 or G^3 position in the *Nar*I recognition sequence.

position	OTB-dG form	rotamer	ΔE_{Hbond} (kcal mol^{-1})[a,b]	ΔE_{vdW} (kcal mol^{-1})[a,c]	shift (Å)[a,d]	slide (Å)[a,d]	rise (Å)[a,d]	tilt (deg.)[a,d]	roll (deg.)[a,d]	twist (deg.)[a,d]	minor groove width (Å)[a,e]
G^1	control	–	–29.0	–30.2	0.1	–0.9	6.6	0.2	11.2	60.7	8.0
	neutral	α	–9.7	–37.4	0.3	–1.2	6.7	4.7	23.5	58.6	8.9
		β	–0.9	–33.8	0.3	–1.4	6.4	1.0	16.1	54.9	8.9
	monoanionic	α	–9.7	–38.3	0.1	–1.5	6.6	2.0	17.2	59.2	8.0
		β	7.9	–32.3	–0.2	–1.9	6.5	-1.4	18.0	53.0	9.1
	dianionic	α	–7.0	–34.8	0.5	–1.2	6.4	2.1	17.9	55.6	9.4
		β	11.0	–31.8	–0.3	–1.4	6.5	-1.8	17.3	54.0	9.4
G^2	control	–	–28.6	–30.9	0.0	–1.2	6.8	0.5	5.0	68.4	7.4
	neutral	α	–10.0	–36.7	1.1	–0.1	6.9	5.4	14.8	68.2	8.4
		β	4.7	–36.9	–0.1	0.0	6.1	1.0	2.7	66.9	7.8
	monoanionic	α	0.9	–29.3	–0.4	0.1	6.1	0.3	10.7	60.6	9.4
		β	9.0	–30.1	–0.4	0.1	6.2	1.9	7.0	65.2	9.0
	dianionic	α	3.9	–29.0	–0.4	0.1	6.2	0.0	13.4	58.9	9.8
		β	11.4	–18.2	–0.4	0.0	6.2	1.6	8.7	63.6	9.6

G^3	control	–	–28.8	–30.7	0.3	–1.0	6.5	2.0	9.8	64.0	7.8
	neutral	α	–2.0	–32.2	–0.1	–0.6	6.2	2.2	12.6	56.9	9.0
		β	–5.8	–34.5	–0.2	–1.5	6.1	3.0	13.8	56.4	9.0
	monoanionic	α	–10.9	–38.4	–0.1	–1.6	6.5	4.0	17.0	61.1	7.6
		β	10.4	–33.0	–0.0	–1.1	6.3	3.4	10.2	58.0	8.8
	dianionic	α	-9.0	–31.4	0.0	–1.5	6.5	2.3	16.8	59.5	8.2
		β	8.8	–19.9	–0.3	–1.2	6.3	3.1	11.3	57.5	9.0

[a]Average calculated from 80000 frames; each frame recorded every 0.5 ps over the 40 ns MD trajectory. [b]Electrostatic interaction energy between the nucleobases forming the Hoogsteen pair at the lesion site. Values for the natural DNA forming Watson-Crick pair are also provided. [c]van der Waals interaction energy between the base pair at the lesion site and the flanking base pairs. [d]Calculated by defining a pseudostep consisting of the two base pairs on the 5′- and 3′-side of the adducted pair. [e]Calculated as the distance between the phosphate atom in the 6^{th} and 23^{rd} residues when the adduct is at G^1, the 7^{th} and 22^{nd} residues when the adduct is at G^2, and the 9^{th} residue and the 20^{th} residue when the adduct is at G^3. The residue numbering within the duplex start from the 5′-end of the adducted strand, and runs from the 3′- to 5′-end of the opposing strand (Figure 1).

Table S3. Salient structural and energetic features of the base-displaced conformations of OTB-dG adducted DNA in the neutral, monoanionic or dianionic OTA ionization state at the G^1, G^2 or G^3 position in the *Nar*I recognition sequence.

position	OTB-dG form	rotamer	ΔE_{vdW} (kcal mol^{-1})[a,b]	shift (Å)[a,c]	slide (Å)[a,c]	rise (Å)[a,c]	tilt (deg.)[a,c]	roll (deg.)[a,c]	twist (deg.)[a,c]	minor groove width (Å)[a,d]
G^1	control	–	–30.2	0.1	-0.9	6.6	0.2	11.2	60.7	8.0
	neutral	α	–38.0	0.7	–0.4	7.0	–1.1	13.5	24.1	11.3
		β	–39.4	0.5	0.9	6.9	1.0	16.1	35.3	11.4
	monoanionic	α	–37.2	0.2	–0.7	7.3	–0.2	15.3	35.4	9.9
		β	–38.4	0.2	1.3	7.2	–0.8	16.5	36.6	11.1
	dianionic	α	–36.2	1.1	–0.1	7.3	4.7	13.5	40.4	10.8
		β	–35.7	–0.2	1.2	7.7	1.1	21.4	34.6	11.4
G^2	control	–	–30.9	0.0	–1.2	6.8	0.5	5.0	68.4	7.4
	neutral	α	–33.1	–0.3	0.0	6.8	–1.8	7.1	48.6	9.5
		β	–37.8	–0.3	1.7	6.5	–2.3	9.5	32.6	12.3
	monoanionic	α	–33.6	–0.5	1.0	6.8	–1.7	9.2	40.1	11.5
		β	–37.6	0.0	1.4	6.6	1.1	11.5	34.8	12.2
	dianionic	α	–32.3	–0.7	1.3	6.8	–2.0	12.8	37.3	12.3

		β	–36.4	0.1	1.4	7.1	2.4	11.1	43.9	11.2
G^3	control	–	–30.7	0.3	–1.0	6.5	2.0	9.8	64.0	7.8
	neutral	α	–35.7	1.2	–2.5	7.2	7.2	14.8	63.9	7.5
		β	–39.5	0.1	1.4	6.9	3.4	16.0	39.3	10.8
	monoanionic	α	–35.4	1.1	–2.8	7.2	5.5	14.1	62.2	7.8
		β	–28.9	0.3	1.0	6.9	3.5	16.4	39.1	10.7
	dianionic	α	–33.4	–0.7	0.5	7.0	0.4	10.8	42.3	11.0
		β	–34.6	–0.3	–0.7	7.3	–1.8	18.2	37.1	10.3

[a]Average value calculated from 80000 frames, with each frame recorded every 0.5 ps over the entire 40 ns MD trajectory. [b]van der Waals interaction energy between the base pair at the lesion site and the flanking base pairs. [c]Calculated by defining a pseudostep consisting of the two base pairs on the 5′- and 3′-side of the adducted pair. [d]Calculated as the distance between the phosphate atom in the 6^{th} and 23^{rd} residues when the adduct is at G^1, the 7^{th} and 22^{nd} residues when the adduct is at G^2, and the 9^{th} residue and the 20^{th} residue when the adduct is at G^3. The residue numbering within the duplex start from the 5′-end of the adducted strand, and runs from the 3′- to 5′-end of the opposing strand (Figure 1).

Table S4. Occupancies of the Watson-Crick hydrogen bonds in the trimers composed of the damaged base pair and the base pairs on the 3′ and 5′ side of the lesion.[a]

			neutral		monoanionic		dianionic		
Sequence	Base Pair	Hydrogen Bond (D–A)	Major groove (α) (%)	Major groove (β) (%)	Major groove (α) (%)	Major groove (β) (%)	Major groove (α) (%)	Major groove (β) (%)	Unmod (%)
5′–CG[1]G–3′	5′C:G	N4(C) – O6(G)	97.8	99.3	97.5	98.5	97.5	99.2	98.7
		N1(G) – N3(C)	100.0	100.0	100.0	100.0	99.8	100.0	100.0
		N2(G) – O2(C)	99.8	99.8	99.8	99.9	99.8	99.8	99.9
	G[1]:C	N4(C) – O6(G)	98.2	98.5	98.4	98.3	98.1	96.4	99.1
		N1(G) – N3(C)	100.0	100.0	100.0	100.0	99.9	97.7	100.0
		N2(G) – O2(C)	99.8	99.9	99.7	99.9	99.7	98.1	99.9
	3′G:C	N4(C) – O6(G)	98.6	98.8	98.3	98.7	98.2	98.5	98.7
		N1(G) – N3(C)	100.0	100.0	100.0	100.0	100.0	99.8	99.9
		N2(G) – O2(C)	99.9	99.9	99.9	99.9	99.9	99.9	99.8
5′–GG[2]C–3′	5′G:C	N4(C) – O6(G)	99.2	98.7	99.2	98.7	98.4	98.4	99.1
		N1(G) – N3(C)	100.0	100.0	100.0	99.9	99.9	99.9	100.0
		N2(G) – O2(C)	99.9	99.9	99.9	99.9	99.7	99.9	99.9
	G[2]:C	N4(C) – O6(G)	98.9	99.4	98.9	99.3	99.1	99.3	98.7
		N1(G) – N3(C)	99.9	100.0	99.9	100.0	99.7	99.9	99.9
		N2(G) – O2(C)	99.9	99.9	98.5	99.7	96.5	99.7	99.8
	3′C:G	N4(C) – O6(G)	99.0	98.9	98.9	99.1	99.1	99.0	98.9
		N1(G) – N3(C)	99.9	100.0	100.0	100.0	100.0	100.0	100.0
		N2(G) – O2(C)	99.9	99.9	99.9	99.9	99.9	99.9	99.9

5′–CG[3]C–3′	5′C:G	N4(C) – O6(G)	99.1	99.3	98.6	99.3	97.9	99.3	98.9
		N1(G) – N3(C)	100.0	100.0	99.9	100.0	99.9	100.0	100.0
		N2(G) – O2(C)	99.8	99.9	99.8	99.9	99.9	99.9	99.9
	G[3]:C	N4(C) – O6(G)	98.5	99.0	98.2	98.9	98.7	99.1	99.1
		N1(G) – N3(C)	100.0	100.0	99.9	99.9	99.9	99.9	100.0
		N2(G) – O2(C)	99.9	99.9	99.2	99.9	99.9	997	99.9
	3′C:G	N4(C) – O6(G)	98.5	98.1	98.6	98.1	99.0	98.2	98.6
		N1(G) – N3(C)	99.9	100.0	100.0	100.0	100.0	100.0	100.0
		N2(G) – O2(C)	99.9	99.9	99.9	99.6	99.9	100.0	99.9

[a]Hydrogen-bond distance cutoff is within 3.40 Å heavy atom separation and 120° X-H-X angle.

Table S5. Occupancies of the Hoogsteen hydrogen bonds at the lesion site and the Watson-Crick hydrogen bonds for the 3′ and 5′ flanking pairs.[a]

			neutral		monoanionic		dianionic		
Sequence	Base Pair	Hydrogen Bond (D–A)	Wedge (α) (%)	Wedge (β) (%)	Wedge (α) (%)	Wedge (β) (%)	Wedge (α) (%)	Wedge (β) (%)	Unmod (%)
	5′C:G	N4(C) – O6(G)	98.7	98.9	98.3	98.4	98.5	98.1	98.7
		N1(G) – N3(C)	99.9	99.9	99.9	99.9	99.4	99.9	100.0
		N2(G) – O2(C)	99.6	99.0	99.6	99.6	96.8	99.7	99.9
	G[1]:C	N4(C) – O6(G)	67.2	62.9	79.6	97.7	96.2	94.6	99.1

5′–CG[1]G–3′		N1(G) – N3(C)	0.0	0.0	0.0	0.0	0.0	0.0	100.0
		N2(G) – O2(C)	0.0	0.0	0.0	0.0	0.0	0.0	99.9
		N4(C) – N7(G)	15.4	11.5	34.9	0.0	50.0	0.0	0.0
	3′G:C	N4(C) – O6(G)	97.7	98.0	96.6	98.8	97.3	98.9	98.7
		N1(G) – N3(C)	99.9	99.8	99.8	99.9	99.8	99.9	99.9
		N2(G) – O2(C)	99.8	99.7	99.8	99.7	99.8	99.8	99.8
5′–GG[2]C–3′	5′G:C	N4(C) – O6(G)	97.0	83.0	95.4	91.1	95.4	92.2	99.1
		N1(G) – N3(C)	99.8	99.7	99.9	99.6	99.8	99.7	100.0
		N2(G) – O2(C)	99.4	99.2	99.8	99.8	99.8	99.8	99.9
	G[2]:C	N4(C) – O6(G)	73.4	11.0	98.0	87.3	98.1	93.7	98.7
		N1(G) – N3(C)	0.0	0.0	0.0	0.0	0.0	0.0	99.9
		N2(G) – O2(C)	0.0	0.0	0.0	0.0	0.0	0.0	99.8
		N4(C) – N7(G)	9.9	0.0	0.0	0.0	0.0	0.0	0.0
	3′C:G	N4(C) – O6(G)	94.4	93.7	97.7	94.2	97.2	95.4	98.9
		N1(G) – N3(C)	98.5	99.7	99.6	99.9	99.8	99.9	100.0
		N2(G) – O2(C)	97.6	97.8	98.9	99.3	99.1	99.3	99.9
5′–CG[3]C–3′	5′C:G	N4(C) – O6(G)	99.1	99.4	98.7	98.3	98.8	98.4	98.9
		N1(G) – N3(C)	100.0	100.0	99.9	99.9	99.7	99.9	100.0
		N2(G) – O2(C)	99.4	99.5	99.9	99.9	99.2	99.8	99.9
	G[3]:C	N4(C) – O6(G)	89.8	87.8	97.5	89.4	98.9	96.2, 35.8	99.1
		N1(G) – N3(C)	0.0	0.0	0.0	0.0	0.0	0.0	100.0
		N2(G) – O2(C)	0.0	0.0	0.0	0.0	0.0	0.0	99.9
		N4(C) – N7(G)	0.0	11.5	14.0	0.0	21.0	0.0	0.0

	3′C:G	N4(C) – O6(G)	98.5	97.6	96.5	95.3	97.1	96.2	98.6
		N1(G) – N3(C)	99.8	99.9	99.7	99.8	99.5	99.8	100.0
		N2(G) – O2(C)	99.0	99.6	97.6	99.5	98.5	99.4	99.9

[a]Hydrogen-bond distance cutoff is within 3.40 Å heavy atom separation and 120° X-H-X angle.

Table S6. Occupancies of the interstrand hydrogen bonds in the trimers composed of the damaged base pair and the adjacent base pairs at the 3′ and 5′ side of the lesion.[a]

			neutral		monoanionic		dianionic		
Sequence	Base Pair	Hydrogen Bond (D–A)	BDS1 (%)	BDS2 (%)	BDS1 (%)	BDS2 (%)	BDS1 (%)	BDS2 (%)	Unmod (%)
5′–CG[1]G–3′	5′C:G	N4(C) – O6(G)	97.1	97.4	98.1	97.3	98.4	97.4	98.7
		N1(G) – N3(C)	99.9	99.9	100.0	99.9	100.0	99.9	100.0
		N2(G) – O2(C)	99.9	99.6	99.7	99.5	98.9	99.4	99.9
	G[1]:C	N4(C) – O6(G)	0.0	0.0	0.0	0.0	0.0	0.0	99.1
		N1(G) – N3(C)	0.0	0.0	0.0	0.0	0.0	0.0	100.0
		N2(G) – O2(C)	0.0	0.0	0.0	0.0	0.0	0.0	99.9
		N4(C) – N7(G)	0.0	0.0	0.0	0.0	0.0	0.0	0.0
	3′G:C	N4(C) – O6(G)	98.7	96.4	98.4	97.3	99.1	98.2	98.7
		N1(G) – N3(C)	99.9	98.1	99.8	99.8	100.0	99.9	99.9
		N2(G) – O2(C)	100.0	99.9	100.0	99.9	99.9	99.9	99.8
5′–GG[2]C–3′	5′G:C	N4(C) – O6(G)	99.9	96.2	97.3	98.2	97.9	98.3	99.1
		N1(G) – N3(C)	100.0	99.9	99.9	99.9	99.9	99.9	100.0

		N2(G) – O2(C)	98.0	99.9	99.8	99.9	9.8	99.8	99.9
	G^2:C	N4(C) – O6(G)	0.0	0.0	0.0	0.0	0.0	0.0	98.7
		N1(G) – N3(C)	0.0	0.0	0.0	0.0	0.0	0.0	99.9
		N2(G) – O2(C)	0.0	0.0	0.0	0.0	0.0	0.0	99.8
		N4(C) – N7(G)	0.0	0.0	0.0	0.0	0.0	0.0	0.0
	3′C:G	N4(C) – O6(G)	99.1	99.0	99.5	98.4	99.9	98.9	98.9
		N1(G) – N3(C)	100.0	100.0	100.0	99.9	100.0	99.9	100.0
		N2(G) – O2(C)	100.0	100.0	100.0	100.0	99.9	100.0	99.9
5′–CG^3C–3′	5′C:G	N4(C) – O6(G)	99.1	98.7	99.3	97.5	97.8	97.4	98.9
		N1(G) – N3(C)	100.0	99.9	100.0	100.0	99.9	100.0	100.0
		N2(G) – O2(C)	99.9	99.9	99.9	99.9	99.7	99.8	99.9
	G^3:C	N4(C) – O6(G)	0.0	0.0	0.0	0.0	0.0	0.0	99.1
		N1(G) – N3(C)	0.0	0.0	0.0	0.0	0.0	0.0	100.0
		N2(G) – O2(C)	0.0	0.0	0.0	0.0	0.0	0.0	99.9
	3′C:G	N4(C) – N7(G)	0.0	0.0	0.0	0.0	0.0	0.0	0.0
		N4(C) – O6(G)	99.0	69.6	98.7	96.7	99.1	97.3	98.6
		N1(G) – N3(C)	100.0	76.2	99.9	99.8	100.0	99.8	100.0
		N2(G) – O2(C)	99.9	69.6	99.8	100.0	99.9	99.9	99.9

[a]Hydrogen bond distance cut-off within 3.40 Å heavy atom separation and 120° X-H-X angle

Table S7. Hydrogen-bond occupancies for the base pairs at the terminal ends of the natural and OTB-dG modified *Nar*I helices.[a]

			C1:G24 pair		C12:G13 pair	
Position	ionization state of OTA	conformer (rotamer)	bond	occupancy	bond	occupancy
	neutral	major groove (α)	N4-H(C)…O6(G)	92.7	N4-H(C)…O6(G)	97.4
			N1-H(G)…N3(C)	97.1	N1-H(G)…N3(C)	99.5
			N2-H(G)…O2(C)	96.1	N2-H(G)…O2(C)	99.6
		major groove (β)	N4-H(C)…O6(G)	97.4	N4-H(C)…O6(G)	97.2
			N1-H(G)…N3(C)	99.9	N1-H(G)…N3(C)	99.3
			N2-H(G)…O2(C)	99.6	N2-H(G)…O2(C)	99.6
		wedge (α)	N4-H(C)…O6(G)	95.9	N4-H(C)…O6(G)	97.5
			N1-H(G)…N3(C)	99.8	N1-H(G)…N3(C)	99.2
			N2-H(G)…O2(C)	99.4	N2-H(G)…O2(C)	99.3
		wedge (β)	N4-H(C)…O6(G)	74.1	N4-H(C)…O6(G)	97.5
			N1-H(G)…N3(C)	85.8	N1-H(G)…N3(C)	99.6
			N2-H(G)…O2(C)	90.8	N2-H(G)…O2(C)	99.6
		base-displaced intercalated (α)	N4-H(C)…O6(G)	95.3	N4-H(C)…O6(G)	97.1
			N1-H(G)…N3(C)	98.5	N1-H(G)…N3(C)	99.1

G^1			N2-H(G)…O2(C)	98.4	N2-H(G)…O2(C)	99.6
		base-displaced intercalated (β)	N4-H(C)…O6(G)	97.5	N4-H(C)…O6(G)	97.6
			N1-H(G)…N3(C)	99.9	N1-H(G)…N3(C)	99.6
			N2-H(G)…O2(C)	99.4	N2-H(G)…O2(C)	99.5
	monoanionic	major groove (α)	N4-H(C)…O6(G)	91.0	N4-H(C)…O6(G)	97.6
			N1-H(G)…N3(C)	98.3	N1-H(G)…N3(C)	99.6
			N2-H(G)…O2(C)	97.8	N2-H(G)…O2(C)	99.6
		major groove (β)	N4-H(C)…O6(G)	93.6	N4-H(C)…O6(G)	97.7
			N1-H(G)…N3(C)	99.1	N1-H(G)…N3(C)	99.6
			N2-H(G)…O2(C)	98.3	N2-H(G)…O2(C)	99.5
		wedge (α)	N4-H(C)…O6(G)	76.4	N4-H(C)…O6(G)	97.2
			N1-H(G)…N3(C)	82.9	N1-H(G)…N3(C)	99.2
			N2-H(G)…O2(C)	85.0	N2-H(G)…O2(C)	99.5
		wedge (β)	N4-H(C)…O6(G)	95.9	N4-H(C)…O6(G)	97.1
			N1-H(G)…N3(C)	98.3	N1-H(G)…N3(C)	99.4
			N2-H(G)…O2(C)	98.0	N2-H(G)…O2(C)	99.5
			N4-H(C)…O6(G)	31.4	N4-H(C)…O6(G)	96.7

		base-displaced intercalated (α)	N1-H(G)…N3(C)	32.4	N1-H(G)…N3(C)	98.4
			N2-H(G)…O2(C)	32.5	N2-H(G)…O2(C)	99.1
			N2-H(G)…N3(G)	51.0	-	-
			N1-H(G)…N3(C)	24.6	-	-
		base-displaced intercalated (β)	N4-H(C)…O6(G)	96.8	N4-H(C)…O6(G)	96.8
			N1-H(G)…N3(C)	99.4	N1-H(G)…N3(C)	98.7
			N2-H(G)…O2(C)	99.3	N2-H(G)…O2(C)	99.3
	dianionic	major groove (α)	N4-H(C)…O6(G)	93.0	N4-H(C)…O6(G)	96.5
			N1-H(G)…N3(C)	99.9	N1-H(G)…N3(C)	98.5
			N2-H(G)…O2(C)	99.0	N2-H(G)…O2(C)	99.2
		major groove (β)	N4-H(C)…O6(G)	94.2	N4-H(C)…O6(G)	97.3
			N1-H(G)…N3(C)	98.2	N1-H(G)…N3(C)	99.3
			N2-H(G)…O2(C)	97.4	N2-H(G)…O2(C)	99.6
		wedge (α)	N4-H(C)…O6(G)	94.5	N4-H(C)…O6(G)	97.4
			N1-H(G)…N3(C)	97.6	N1-H(G)…N3(C)	99.3
			N2-H(G)…O2(C)	97.0	N2-H(G)…O2(C)	99.4
			N4-H(C)…O6(G)	95.2	N4-H(C)…O6(G)	46.8

		wedge (β)	N1-H(G)…N3(C)	98.6	N1-H(G)…N3(C)	48.8
			N2-H(G)…O2(C)	99.1	N2-H(G)…O2(C)	48.2
		base-displaced intercalated (α)	N4-H(C)…O6(G)	92.7	N4-H(C)…O6(G)	97.0
			N1-H(G)…N3(C)	95.2	N1-H(G)…N3(C)	99.1
			N2-H(G)…O2(C)	94.6	N2-H(G)…O2(C)	99.5
		base-displaced intercalated (β)	N4-H(C)…O6(G)	97.4	N4-H(C)…O6(G)	97.1
			N1-H(G)…N3(C)	99.6	N1-H(G)…N3(C)	99.0
			N2-H(G)…O2(C)	99.3	N2-H(G)…O2(C)	99.5
	neutral	major groove (α)	N4-H(C)…O6(G)	96.1	N4-H(C)…O6(G)	97.3
			N1-H(G)…N3(C)	99.5	N1-H(G)…N3(C)	99.3
			N2-H(G)…O2(C)	99.0	N2-H(G)…O2(C)	99.5
		major groove (β)	N4-H(C)…O6(G)	95.8	N4-H(C)…O6(G)	97.2
			N1-H(G)…N3(C)	98.8	N1-H(G)…N3(C)	99.4
			N2-H(G)…O2(C)	98.4	N2-H(G)…O2(C)	99.6
		wedge (α)	N4-H(C)…O6(G)	94.4	N4-H(C)…O6(G)	96.5
			N1-H(G)…N3(C)	99.1	N1-H(G)…N3(C)	98.7
			N2-H(G)…O2(C)	97.9	N2-H(G)…O2(C)	99.4

		wedge (β)	N4-H(C)…O6(G)	93.4	N4-H(C)…O6(G)	54.8
			N1-H(G)…N3(C)	98.2	N1-H(G)…N3(C)	56.9
			N2-H(G)…O2(C)	98.7	N2-H(G)…O2(C)	61.3
		base-displaced intercalated (α)	N4-H(C)…O6(G)	95.9	N4-H(C)…O6(G)	97.4
			N1-H(G)…N3(C)	99.0	N1-H(G)…N3(C)	99.4
			N2-H(G)…O2(C)	98.4	N2-H(G)…O2(C)	99.6
		base-displaced intercalated (β)	N4-H(C)…O6(G)	96.7	N4-H(C)…O6(G)	97.2
			N1-H(G)…N3(C)	99.9	N1-H(G)…N3(C)	99.3
			N2-H(G)…O2(C)	99.3	N2-H(G)…O2(C)	99.6
	monoanionic	major groove (α)	N4-H(C)…O6(G)	69.5	N4-H(C)…O6(G)	96.0
			N1-H(G)…N3(C)	72.3	N1-H(G)…N3(C)	97.8
			N2-H(G)…O2(C)	72.0	N2-H(G)…O2(C)	99.0
		major groove (β)	N4-H(C)…O6(G)	95.1	N4-H(C)…O6(G)	97.1
			N1-H(G)…N3(C)	99.8	N1-H(G)…N3(C)	99.1
			N2-H(G)…O2(C)	99.3	N2-H(G)…O2(C)	99.6
		wedge (α)	N4-H(C)…O6(G)	95.6	N4-H(C)…O6(G)	97.5
			N1-H(G)…N3(C)	99.8	N1-H(G)…N3(C)	99.1

G^2			N2-H(G)…O2(C)	99.3	N2-H(G)…O2(C)	99.6
		wedge (β)	N4-H(C)…O6(G)	95.6	N4-H(C)…O6(G)	95.8
			N1-H(G)…N3(C)	99.6	N1-H(G)…N3(C)	97.8
			N2-H(G)…O2(C)	99.3	N2-H(G)…O2(C)	98.9
		base-displaced intercalated (α)	N4-H(C)…O6(G)	96.2	N4-H(C)…O6(G)	97.4
			N1-H(G)…N3(C)	99.8	N1-H(G)…N3(C)	99.3
			N2-H(G)…O2(C)	99.2	N2-H(G)…O2(C)	99.6
		base-displaced intercalated (β)	N4-H(C)…O6(G)	96.2	N4-H(C)…O6(G)	95.4
			N1-H(G)…N3(C)	96.2	N1-H(G)…N3(C)	97.4
			N2-H(G)…O2(C)	95.6	N2-H(G)…O2(C)	98.3
	dianionic	major groove (α)	N4-H(C)…O6(G)	80.6	N4-H(C)…O6(G)	79.9
			N1-H(G)…N3(C)	78.9	N1-H(G)…N3(C)	73.0
			N2-H(G)…O2(C)	78.5	N2-H(G)…O2(C)	73.2
		major groove (β)	N4-H(C)…O6(G)	98.6	N4-H(C)…O6(G)	96.5
			N1-H(G)…N3(C)	98.9	N1-H(G)…N3(C)	98.6
			N2-H(G)…O2(C)	99.3	N2-H(G)…O2(C)	96.5
			N4-H(C)…O6(G)	95.6	N4-H(C)…O6(G)	94.5

		wedge (α)	N1-H(G)…N3(C)	99.0	N1-H(G)…N3(C)	96.7
			N2-H(G)…O2(C)	98.5	N2-H(G)…O2(C)	98.3
		wedge (β)	N4-H(C)…O6(G)	96.4	N4-H(C)…O6(G)	97.0
			N1-H(G)…N3(C)	99.9	N1-H(G)…N3(C)	99.2
			N2-H(G)…O2(C)	99.3	N2-H(G)…O2(C)	99.5
		base-displaced intercalated (α)	N4-H(C)…O6(G)	85.0	N4-H(C)…O6(G)	99.2
			N1-H(G)…N3(C)	93.1	N1-H(G)…N3(C)	99.5
			N2-H(G)…O2(C)	96.1	N2-H(G)…O2(C)	97.1
		base-displaced intercalated (β)	N4-H(C)…O6(G)	95.8	N4-H(C)…O6(G)	95.6
			N1-H(G)…N3(C)	99.4	N1-H(G)…N3(C)	97.8
			N2-H(G)…O2(C)	98.7	N2-H(G)…O2(C)	98.2
	neutral	major groove (α)	N4-H(C)…O6(G)	83.3	N4-H(C)…O6(G)	96.4
			N1-H(G)…N3(C)	87.6	N1-H(G)…N3(C)	98.8
			N2-H(G)…O2(C)	87.5	N2-H(G)…O2(C)	99.0
		major groove (β)	N4-H(C)…O6(G)	94.6	N4-H(C)…O6(G)	97.5
			N1-H(G)…N3(C)	99.1	N1-H(G)…N3(C)	99.4
			N2-H(G)…O2(C)	98.7	N2-H(G)…O2(C)	99.6

		wedge (α)	N4-H(C)…O6(G)	95.7	N4-H(C)…O6(G)	97.5
			N1-H(G)…N3(C)	99.8	N1-H(G)…N3(C)	99.4
			N2-H(G)…O2(C)	99.3	N2-H(G)…O2(C)	99.7
		wedge (β)	N4-H(C)…O6(G)	95.4	N4-H(C)…O6(G)	97.1
			N1-H(G)…N3(C)	99.7	N1-H(G)…N3(C)	99.1
			N2-H(G)…O2(C)	99.4	N2-H(G)…O2(C)	99.6
		base-displaced intercalated (α)	N4-H(C)…O6(G)	95.4	N4-H(C)…O6(G)	88.5
			N1-H(G)…N3(C)	99.9	N1-H(G)…N3(C)	90.5
			N2-H(G)…O2(C)	99.4	N2-H(G)…O2(C)	94.4
		base-displaced intercalated (β)	N4-H(C)…O6(G)	95.2	N4-H(C)…O6(G)	97.4
			N1-H(G)…N3(C)	99.4	N1-H(G)…N3(C)	99.3
			N2-H(G)…O2(C)	99.2	N2-H(G)…O2(C)	99.4
	monoanionic	major groove (α)	N4-H(C)…O6(G)	95.5	N4-H(C)…O6(G)	84.8
			N1-H(G)…N3(C)	99.7	N1-H(G)…N3(C)	87.3
			N2-H(G)…O2(C)	99.2	N2-H(G)…O2(C)	91.4
		major groove (β)	N4-H(C)…O6(G)	95.7	N4-H(C)…O6(G)	94.3
			N1-H(G)…N3(C)	99.7	N1-H(G)…N3(C)	96.2

G^3			N2-H(G)…O2(C)	99.2	N2-H(G)…O2(C)	98.2
		wedge (α)	N4-H(C)…O6(G)	95.8	N4-H(C)…O6(G)	97.4
			N1-H(G)…N3(C)	99.1	N1-H(G)…N3(C)	99.5
			N2-H(G)…O2(C)	98.6	N2-H(G)…O2(C)	99.5
		wedge (β)	N4-H(C)…O6(G)	95.4	N4-H(C)…O6(G)	94.6
			N1-H(G)…N3(C)	99.7	N1-H(G)…N3(C)	96.7
			N2-H(G)…O2(C)	99.2	N2-H(G)…O2(C)	98.7
		base-displaced intercalated (α)	N4-H(C)…O6(G)	96.0	N4-H(C)…O6(G)	97.0
			N1-H(G)…N3(C)	98.2	N1-H(G)…N3(C)	99.1
			N2-H(G)…O2(C)	97.7	N2-H(G)…O2(C)	99.6
		base-displaced intercalated (β)	N4-H(C)…O6(G)	70.6	N4-H(C)…O6(G)	96.6
			N1-H(G)…N3(C)	83.8	N1-H(G)…N3(C)	99.2
			N2-H(G)…O2(C)	88.6	N2-H(G)…O2(C)	99.2
	dianionic	major groove (α)	N4-H(C)…O6(G)	95.7	N4-H(C)…O6(G)	97.4
			N1-H(G)…N3(C)	99.9	N1-H(G)…N3(C)	99.5
			N2-H(G)…O2(C)	99.4	N2-H(G)…O2(C)	99.5
			N4-H(C)…O6(G)	95.3	N4-H(C)…O6(G)	96.0

		major groove (β)	N1-H(G)…N3(C)	99.7	N1-H(G)…N3(C)	98.0
			N2-H(G)…O2(C)	99.3	N2-H(G)…O2(C)	98.8
		wedge (α)	N4-H(C)…O6(G)	96.2	N4-H(C)…O6(G)	97.6
			N1-H(G)…N3(C)	99.6	N1-H(G)…N3(C)	99.6
			N2-H(G)…O2(C)	99.0	N2-H(G)…O2(C)	99.6
		wedge (β)	N4-H(C)…O6(G)	95.7	N4-H(C)…O6(G)	95.9
			N1-H(G)…N3(C)	99.8	N1-H(G)…N3(C)	97.9
			N2-H(G)…O2(C)	99.4	N2-H(G)…O2(C)	98.9
		base-displaced intercalated (α)	N4-H(C)…O6(G)	95.5	N4-H(C)…O6(G)	97.5
			N1-H(G)…N3(C)	99.8	N1-H(G)…N3(C)	99.5
			N2-H(G)…O2(C)	99.3	N2-H(G)…O2(C)	99.6
		base-displaced intercalated (β)	N4-H(C)…O6(G)	95.7	N4-H(C)…O6(G)	96.4
			N1-H(G)…N3(C)	99.8	N1-H(G)…N3(C)	98.4
			N2-H(G)…O2(C)	99.4	N2-H(G)…O2(C)	99.3

[a]Hydrogen-bond distance cutoff is within 3.40 Å heavy atom separation and 120° X-H-X angle.

Table S8. Partial charges of the neutral OTB-dG adduct generated using the RED program (atom numbering provided).

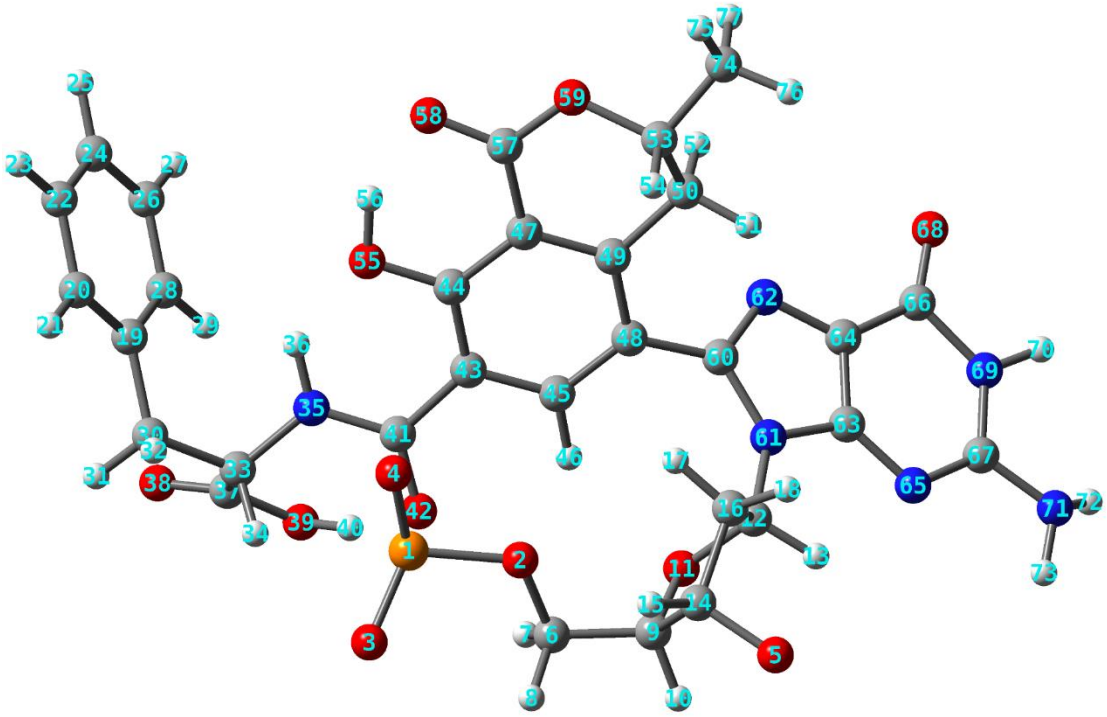

Atom no.	Symbol	Atom type	Atomic charge
1	P	P	1.1706
2	O	OS	-0.4973
3	O	O2	-0.7693
4	O	O2	-0.7693
5	O	OS	-0.544
6	C	CI	-0.0335
7	H	H1	0.0862
8	H	H1	0.0862
9	C	CT	0.1607
10	H	H1	0.0844

11	O	OS	-0.3953
12	C	CT	0.1501
13	H	H2	0.035
14	C	CT	0.173
15	H	H1	0.0625
16	C	CT	-0.0039
17	H	HC	0.0336
18	H	HC	0.0336
19	C	CA	0.0072
20	C	CA	-0.0855
21	H	HA	0.1389
22	C	CA	-0.1933
23	H	HA	0.1489
24	C	CA	-0.1123
25	H	HA	0.1356
26	C	CA	-0.1748
27	H	HA	0.1477
28	C	CA	-0.1147
29	H	HA	0.1101
30	C	CT	-0.101
31	H	HC	0.0629
32	H	HC	0.0629
33	C	CT	-0.0087
34	H	H1	0.0906

35	N	N	-0.2329
36	H	H	0.2161
37	C	C	0.6594
38	O	O	-0.5178
39	O	OH	-0.6158
40	H	HO	0.4385
41	C	C	0.4301
42	O	O	-0.5901
43	C	CA	-0.0215
44	C	CA	0.0799
45	C	CA	-0.0174
46	H	HA	0.1589
47	C	CA	-0.0876
48	C	CA	-0.0181
49	C	CA	-0.085
50	C	CT	-0.0203
51	H	HC	0.0665
52	H	HC	0.0665
53	C	CT	0.3187
54	H	H1	0.0234
55	O	OH	-0.4558
56	H	HO	0.4378
57	C	C	0.7249
58	O	O	-0.5964

59	O	OS	-0.4341
60	C	CK	0.1759
61	N	N*	0.0358
62	N	NB	-0.444
63	C	CB	0.1588
64	C	CB	0.0765
65	N	NC	-0.4179
66	C	C	0.4743
67	C	CA	0.5064
68	O	O	-0.538
69	N	NA	-0.4021
70	H	H	0.3382
71	N	N2	-0.8147
72	H	H	0.38
73	H	H	0.38
74	C	CT	-0.2576
75	H	HC	0.0811
76	H	HC	0.0811
77	H	HC	0.0811

Table S9. Partial charges of the monoanionic (carboxylic group ionized) OTB-dG adduct generated using the RED program (atom numbering provided)**.**

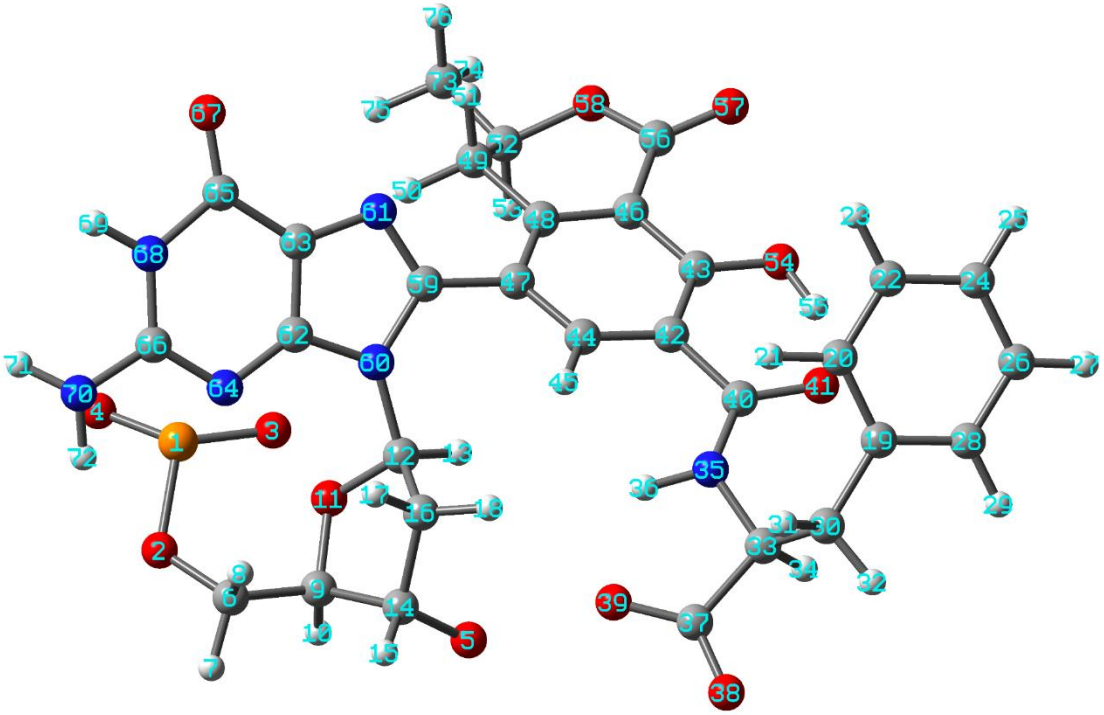

Atom no.	Symbol	Atom type	Atomic charge
1	P	P	1.1658
2	O	OS	-0.5093
3	O	O2	-0.7674
4	O	O2	-0.7674
5	O	OS	-0.5408
6	C	CI	0.0116
7	H	H1	0.073
8	H	H1	0.073
9	C	CT	0.1496
10	H	H1	0.1153
11	O	OS	-0.4216

12	C	CT	-0.0633
13	H	H2	0.2083
14	C	CT	0.1291
15	H	H1	0.0747
16	C	CT	-0.0717
17	H	HC	0.0491
18	H	HC	0.0491
19	C	CA	0.0155
20	C	CA	-0.0912
21	H	HA	0.1453
22	C	CA	-0.1824
23	H	HA	0.1271
24	C	CA	-0.1216
25	H	HA	0.1167
26	C	CA	-0.1793
27	H	HA	0.1342
28	C	CA	-0.186
29	H	HA	0.1598
30	C	CT	-0.0585
31	H	HC	0.0425
32	H	HC	0.0425
33	C	CT	0.0324
34	H	H1	0.0614
35	N	N	-0.2321
36	H	H	0.1873
37	C	C	0.68
38	O	O2	-0.6897
39	O	O2	-0.6865
40	C	C	0.4082
41	O	O	-0.5622
42	C	CA	-0.0299
43	C	CA	0.2541
44	C	CA	-0.2864
45	H	HA	0.227
46	C	CA	-0.1049
47	C	CA	-0.0382
48	C	CA	-0.0806
49	C	CT	-0.0313
50	H	HC	0.0659
51	H	HC	0.0659
52	C	CT	0.3359

53	H	H1	0.0019
54	O	OH	-0.5191
55	H	HO	0.4278
56	C	C	0.7597
57	O	O	-0.5604
58	O	OS	-0.4985
59	C	CK	0.3168
60	N	N*	0.0364
61	N	NB	-0.5346
62	C	CB	0.1063
63	C	CB	0.1361
64	N	NC	-0.375
65	C	C	0.4291
66	C	CA	0.4623
67	O	O	-0.5465
68	N	NA	-0.3501
69	H	H	0.3233
70	N	N2	-0.8095
71	H	H	0.3664
72	H	H	0.3664
73	C	CT	-0.2181
74	H	HC	0.0605
75	H	HC	0.0605
76	H	HC	0.0605

Table S10. Partial charges of the dianionic (carboxylic and phenolic group ionized) OTB-dG adduct generated using the RED program (atom numbering provided)**.**

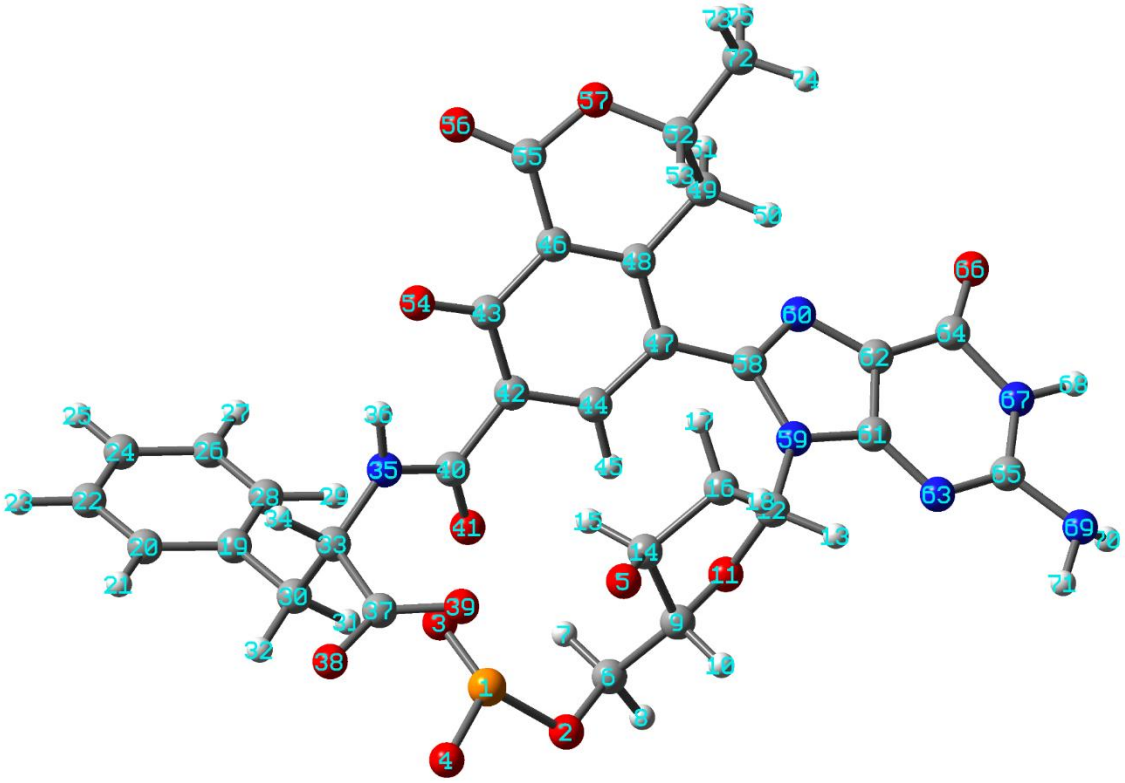

Atom no.	Symbol	Atom type	Atomic charge
1	P	P	1.165
2	O	OS	-0.5277
3	O	O2	-0.7663
4	O	O2	-0.7663
5	O	OS	-0.545
6	C	CI	-0.0142
7	H	H1	0.0857
8	H	H1	0.0857
9	C	CT	0.1445
10	H	H1	0.1083

11	O	OS	-0.413
12	C	CT	-0.0755
13	H	H2	0.1369
14	C	CT	0.1425
15	H	H1	0.0885
16	C	CT	-0.0859
17	H	HC	0.0548
18	H	HC	0.0548
19	C	CA	-0.0311
20	C	CA	-0.1002
21	H	HA	0.1134
22	C	CA	-0.2011
23	H	HA	0.1168
24	C	CA	-0.1414
25	H	HA	0.1071
26	C	CA	-0.169
27	H	HA	0.1256
28	C	CA	-0.1089
29	H	HA	0.146
30	C	CT	-0.1223
31	H	HC	0.0769
32	H	HC	0.0769
33	C	CT	0.0837
34	H	H1	0.0269

35	N	N	-0.1664
36	H	H	0.2006
37	C	C	0.7687
38	O	O2	-0.7572
39	O	O2	-0.7822
40	C	C	0.2756
41	O	O	-0.5437
42	C	CA	-0.0213
43	C	C	0.329
44	C	CA	-0.1793
45	H	HA	0.1654
46	C	CA	-0.2033
47	C	CA	-0.0352
48	C	CA	-0.1103
49	C	CT	-0.0097
50	H	HC	0.0437
51	H	HC	0.0437
52	C	CT	0.3777
53	H	H1	0.001
54	O	O	-0.5876
55	C	C	0.731
56	O	O	-0.5924
57	O	OS	-0.5076
58	C	CK	0.2933

59	N	N*	0.1072
60	N	NB	-0.5975
61	C	CB	0.1587
62	C	CB	0.1077
63	N	NC	-0.567
64	C	C	0.5549
65	C	CA	0.715
66	O	O	-0.5956
67	N	NA	-0.5721
68	H	H	0.3543
69	N	N2	-0.9145
70	H	H	0.377
71	H	H	0.377
72	C	CT	-0.331
73	H	HC	0.0734
74	H	HC	0.0734
75	H	HC	0.0734

Table S11. Average and standard deviation of the backbone RMSD obtained from MD simulations of OTB-dG adducted DNA in three ionization states.

Position	conformer	ionization state of OTA	average RMSD (Å)	standard deviation (Å)
G^1	major groove (α)	neutral	2.050	0.449
	major groove (β)		4.064	0.747
	wedge (α)		3.575	0.722
	wedge (β)		3.751	0.743
	base-displaced intercalated (α)		2.519	0.578
	base-displaced intercalated (β)		2.424	0.403
	major groove (α)	monoanionic	3.740	0.657
	major groove (β)		3.372	0.671
	wedge (α)		2.255	0.460
	wedge (β)		2.352	0.407
	base-displaced intercalated (α)		2.428	0.348
	base-displaced intercalated (β)		2.415	0.382
	major groove (α)		3.266	0.650

	major groove (β)	dianionic	1.907	0.371
	wedge (α)		3.581	0.704
	wedge (β)		3.882	0.671
	base-displaced intercalated (α)		2.598	0.445
	base-displaced intercalated (β)		2.064	0.470
G^2	major groove (α)	neutral	3.769	0.716
	major groove (β)		3.935	0.680
	wedge (α)		2.417	0.550
	wedge (β)		2.820	0.718
	base-displaced intercalated (α)		4.100	0.659
	base-displaced intercalated (β)		3.175	0.594
	major groove (α)	monoanionic	2.888	0.787
	major groove (β)		3.409	0.621
	wedge (α)		2.273	0.479
	wedge (β)		2.332	0.417
	base-displaced intercalated (α)		1.950	0.363
	base-displaced intercalated (β)		2.733	0.488
	major groove (α)	dianionic	3.162	0.692
	major groove (β)		3.961	0.681
	wedge (α)		3.820	0.633
	wedge (β)		2.261	0.449
	base-displaced intercalated (α)		2.023	0.388
	base-displaced intercalated (β)		2.210	0.409

G^3	major groove (α)	neutral	4.069	0.818
	major groove (β)		3.498	0.629
	wedge (α)		2.141	0.416
	wedge (β)		2.025	0.374
	base-displaced intercalated (α)		4.284	0.695
	base-displaced intercalated (β)		2.295	0.417
	major groove (α)	monoanionic	3.613	0.747
	major groove (β)		3.753	0.703
	wedge (α)		2.359	0.412
	wedge (β)		1.897	0.393
	base-displaced intercalated (α)		2.192	0.456
	base-displaced intercalated (β)		2.833	0.416
	major groove (α)	dianionic	3.794	0.682
	major groove (β)		4.102	0.784
	wedge (α)		1.923	0.419
	wedge (β)		2.004	0.393
	base-displaced intercalated (α)		4.635	0.699
	base-displaced intercalated (β)		2.440	0.528

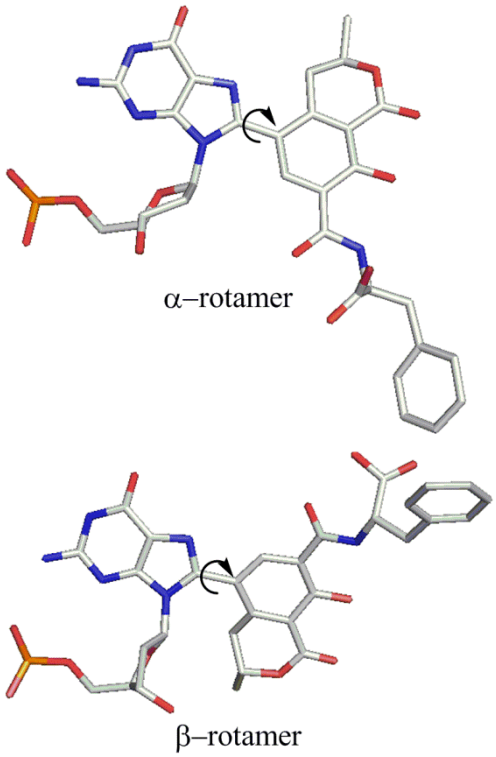

Figure S1. The α and β rotamers of the OTB-dG lesion formed by rotating across the nucleobase-adduct linkage (indicated with round arrows).

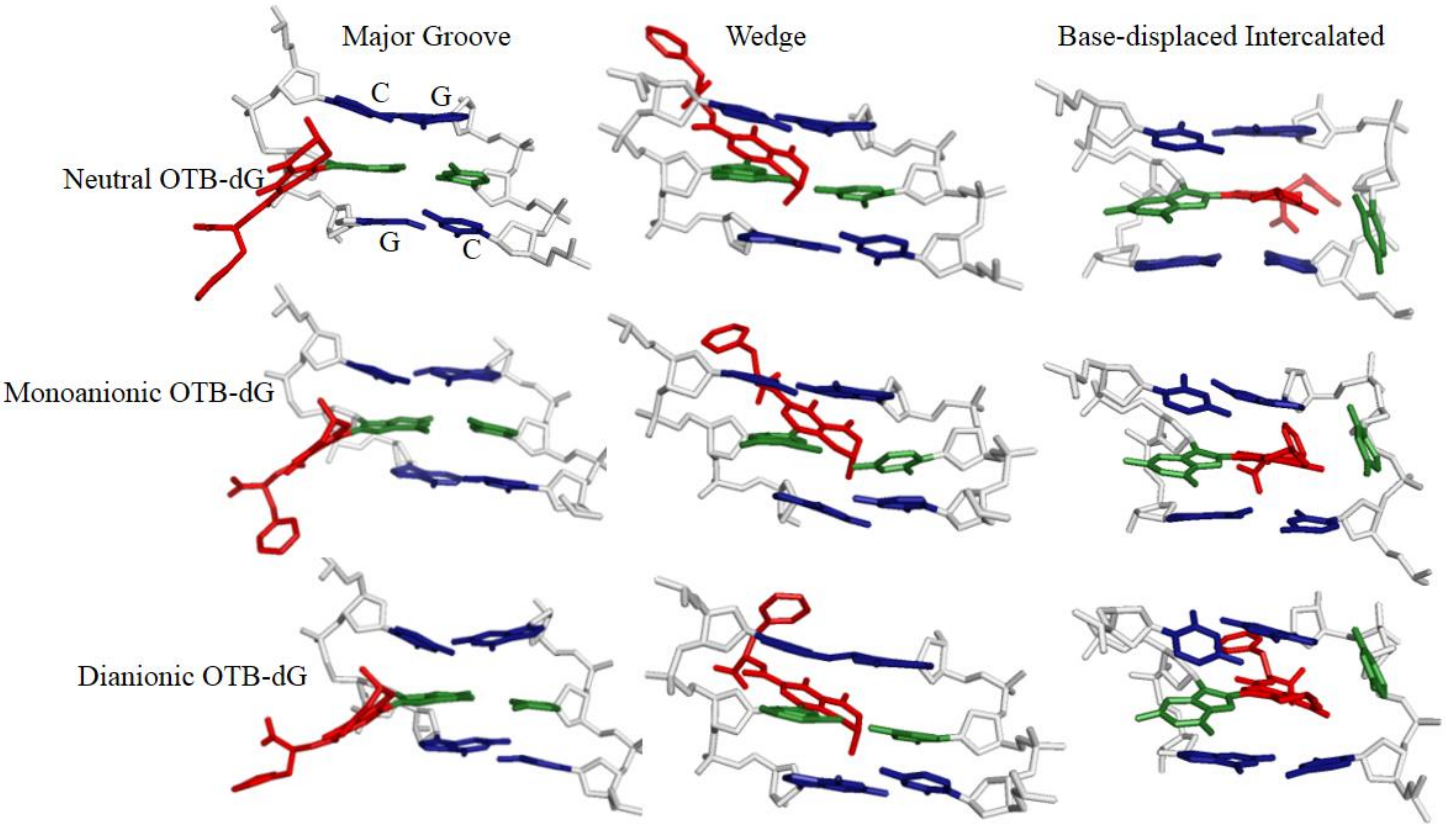

Figure S2. Representative structures of the OTB-dG α-rotamer in various ionization states and the G^1 position in different conformations of the adducted *Nar*I recognition sequence. Central trimers including the lesion (red) base pair (green) and the flanking base pairs (blue) viewed from the major groove side are shown (sugar–phosphate backbone in white). Hydrogen atoms were removed for clarity.

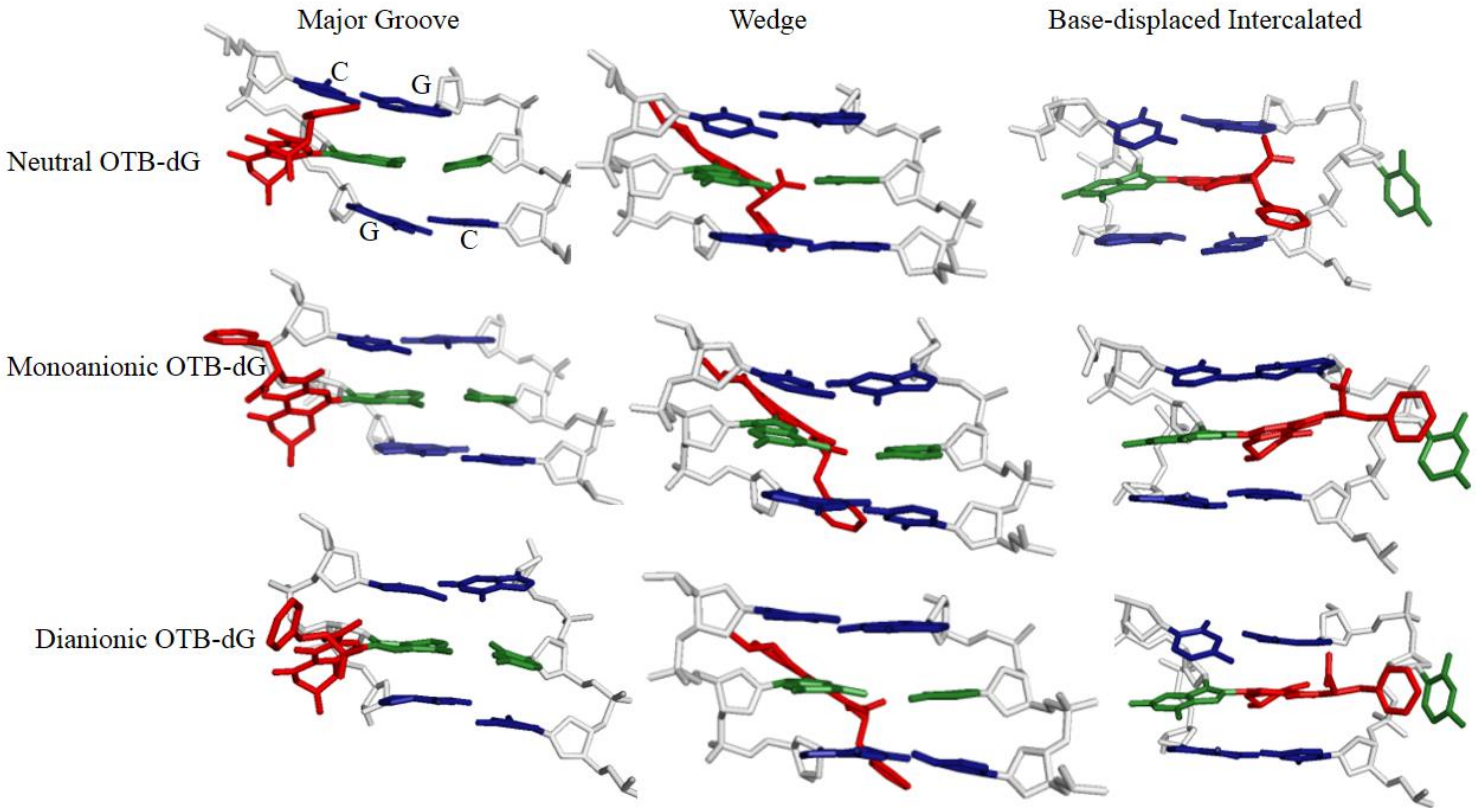

Figure S3. Representative structures of the OTB-dG β-rotamer in various ionization states and the G^1 position in different conformations of the adducted *Nar*I recognition sequence. Central trimers including the lesion (red) base pair (green) and the flanking base pairs (blue) viewed from the major groove side are shown (sugar–phosphate backbone in white). Hydrogen atoms were removed for clarity.

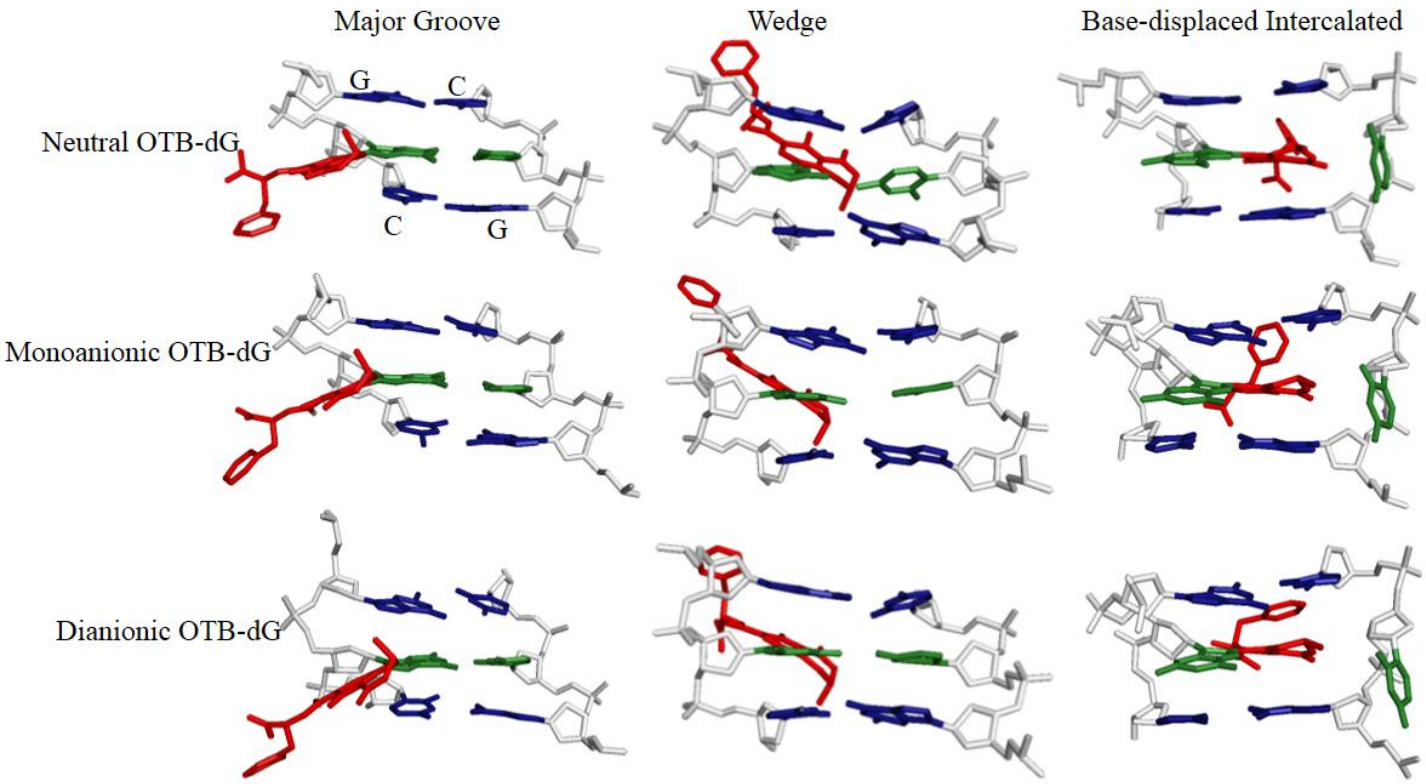

Figure S4. Representative structures of the OTB-dG α-rotamer in various ionization states and the G^2 position in different conformations of the adducted *Nar*I recognition sequence. Central trimers including the lesion (red) base pair (green) and the flanking base pairs (blue) viewed from the major groove side are shown (sugar–phosphate backbone in white). Hydrogen atoms were removed for clarity.

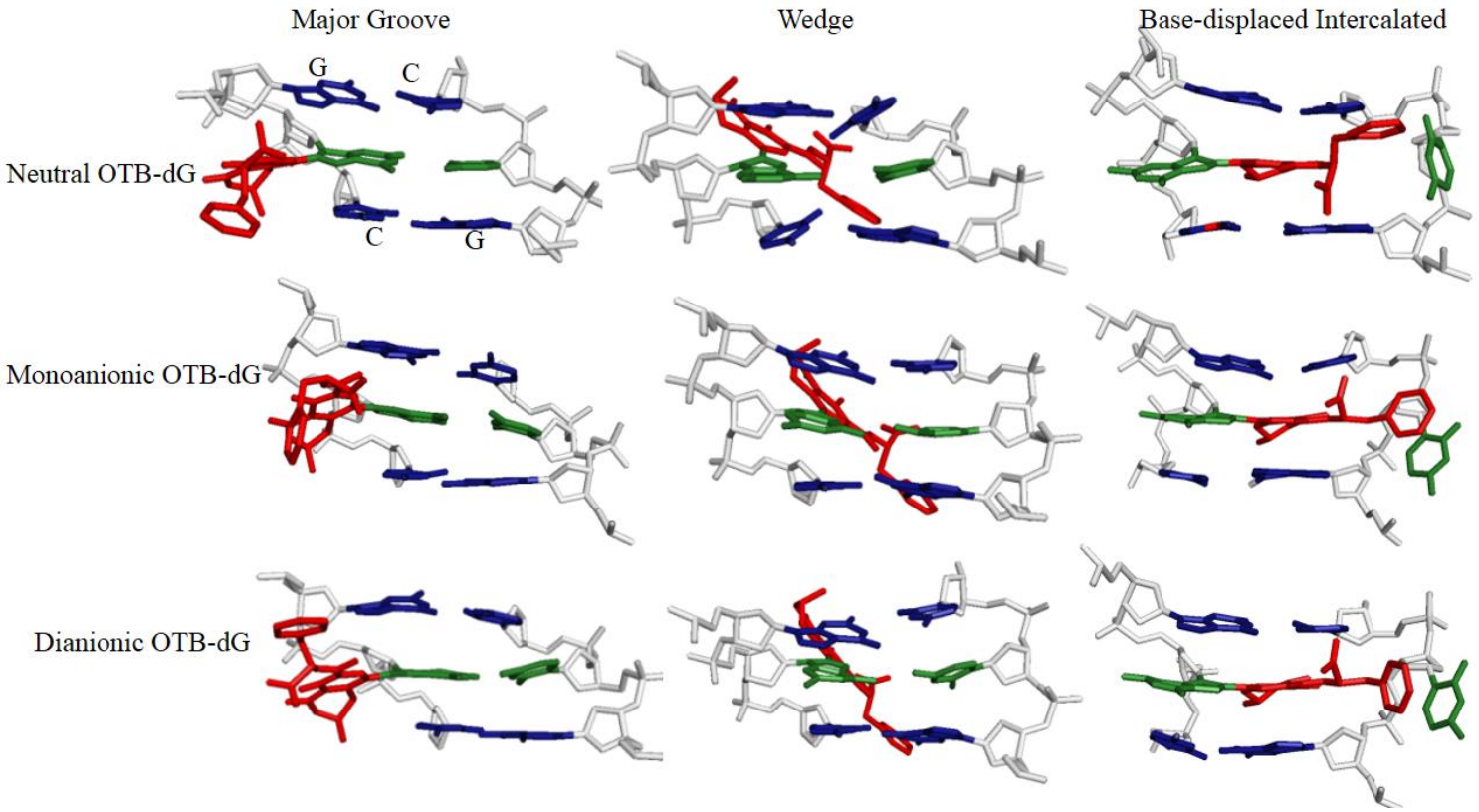

Figure S5. Representative structures of the OTB-dG β-rotamer in various ionization states and the G^2 position in different conformations of the adducted *Nar*I recognition sequence. Central trimers including the lesion (red) base pair (green) and the flanking base pairs (blue) viewed from the major groove side are shown (sugar–phosphate backbone in white). Hydrogen atoms were removed for clarity.

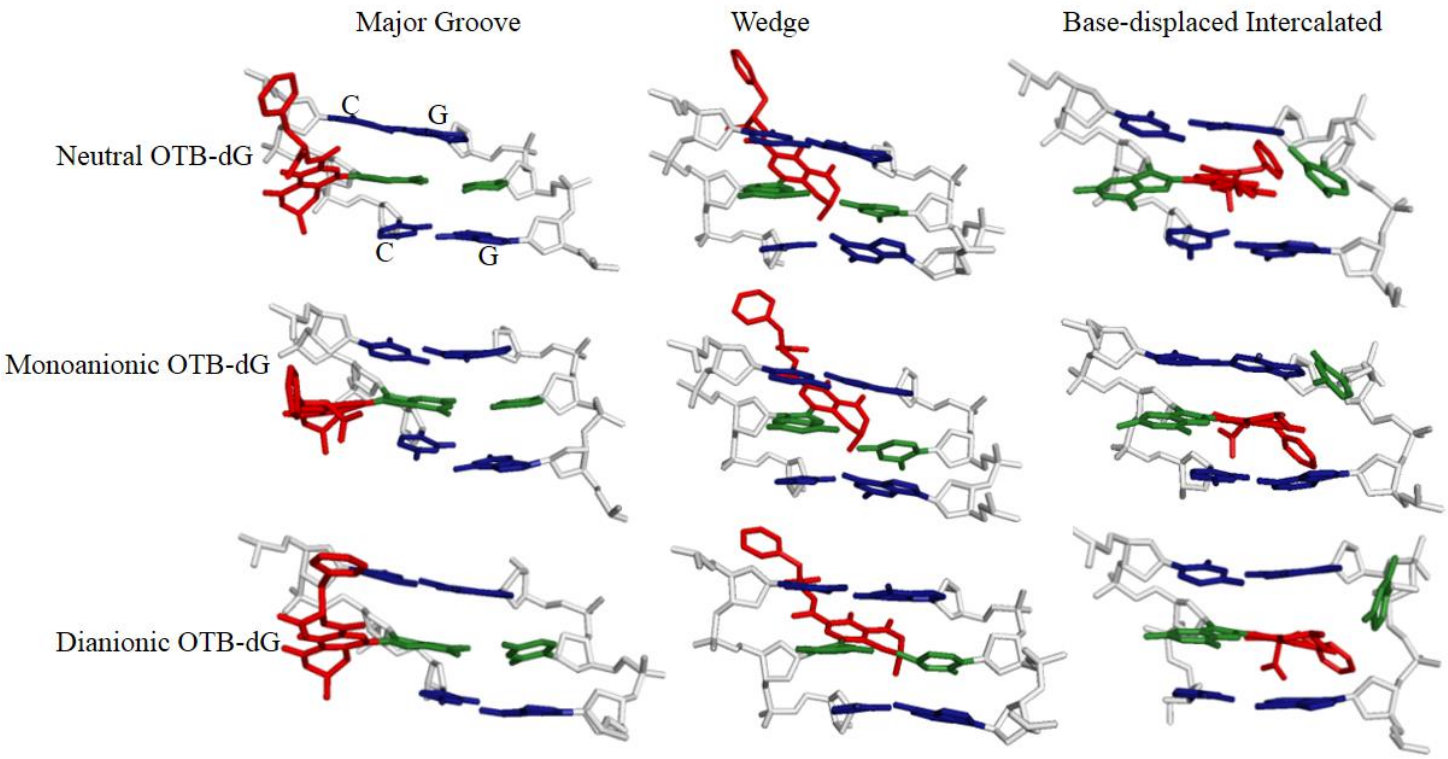

Figure S6. Representative structures of the OTB-dG α-rotamer in various ionization states and the G^3 position in different conformations of the adducted *Nar*I recognition sequence. Central trimers including the lesion (red) base pair (green) and the flanking base pairs (blue) viewed from the major groove side are shown (sugar–phosphate backbone in white). Hydrogen atoms were removed for clarity.

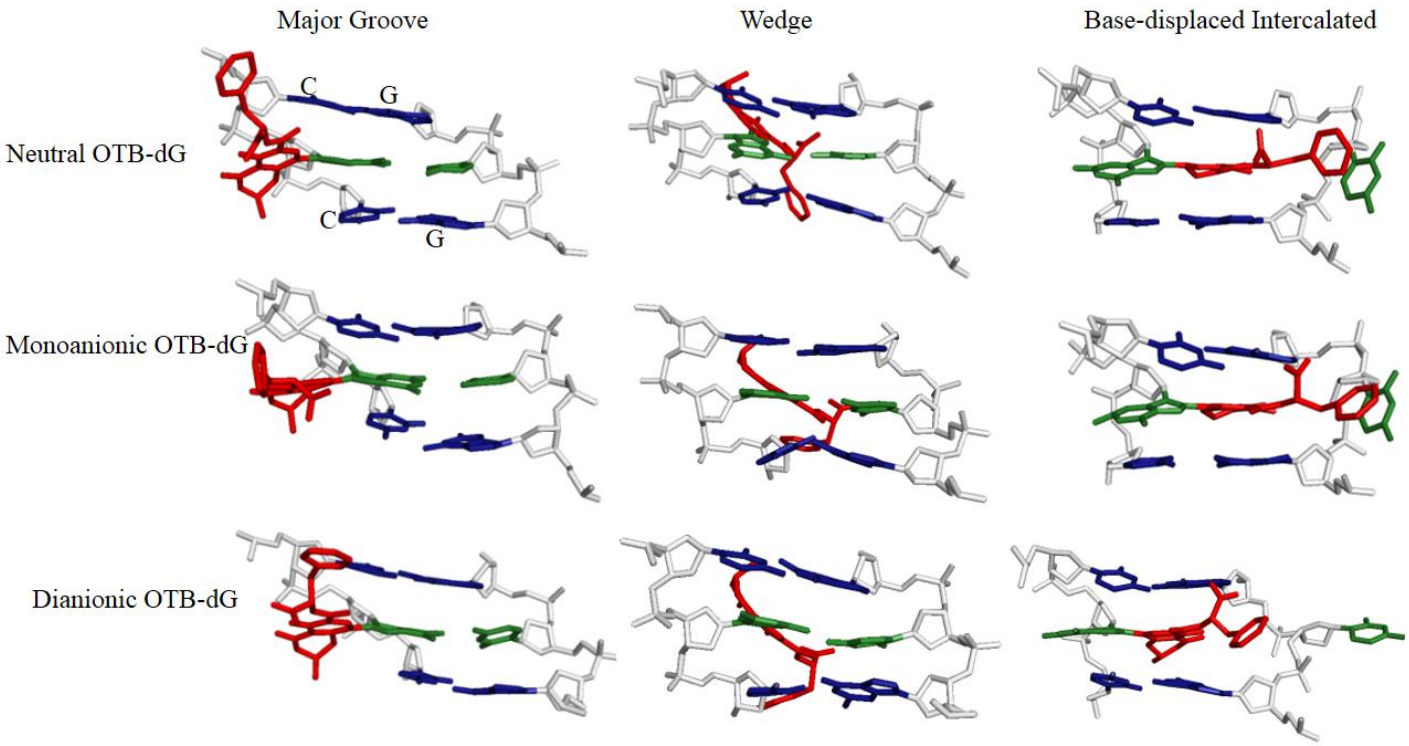

Figure S7. Representative structures of the OTB-dG β-rotamer in various ionization states and the G^3 position in different conformations of the adducted *Nar*I recognition sequence. Central trimers including the lesion (red) base pair (green) and the flanking base pairs (blue) viewed from the major groove side are shown (sugar–phosphate backbone in white). Hydrogen atoms were removed for clarity.

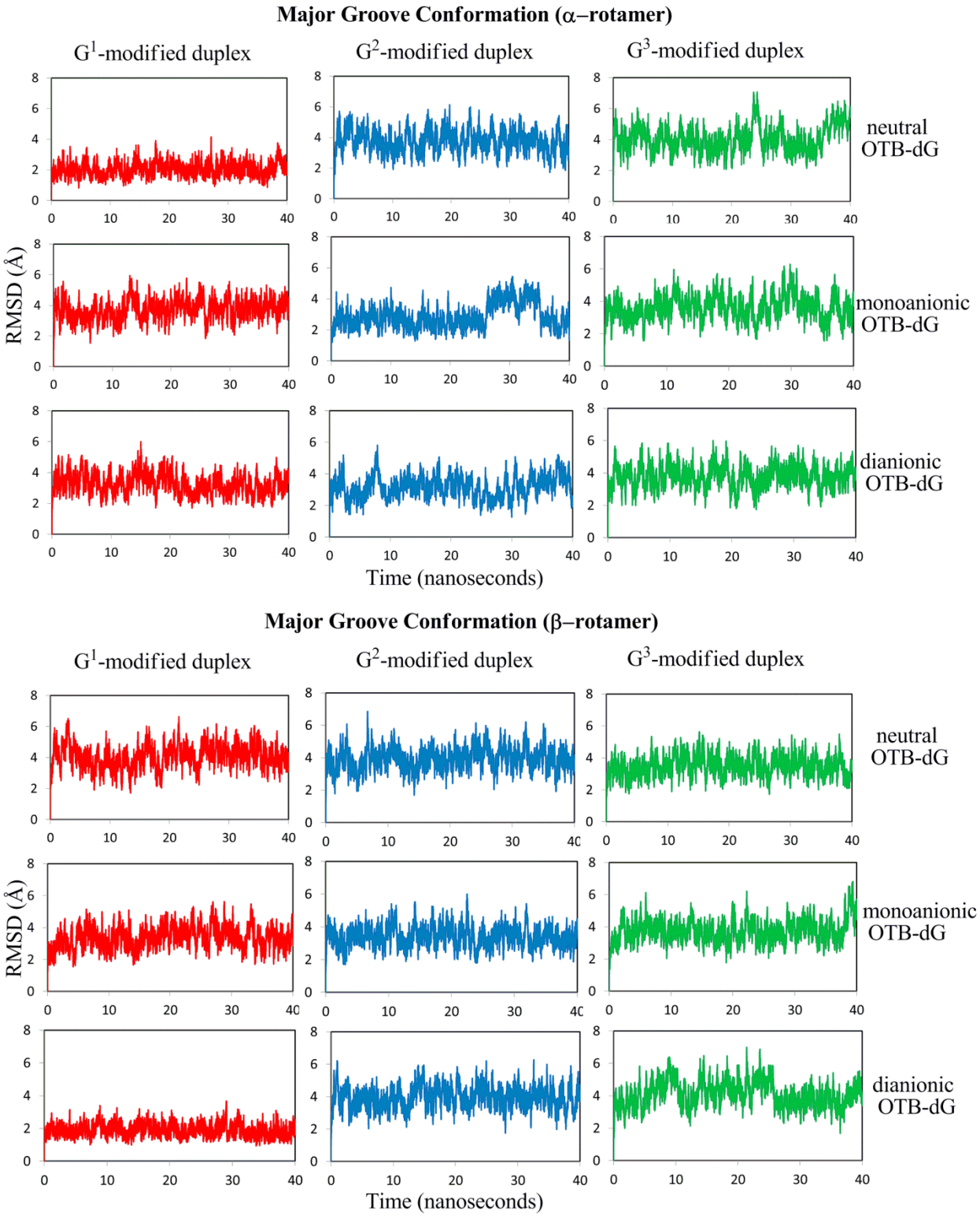

Figure S8. Backbone RMSD versus time for the major groove conformations of OTB-dG adducted DNA with the adduct in three positions and ionization states.

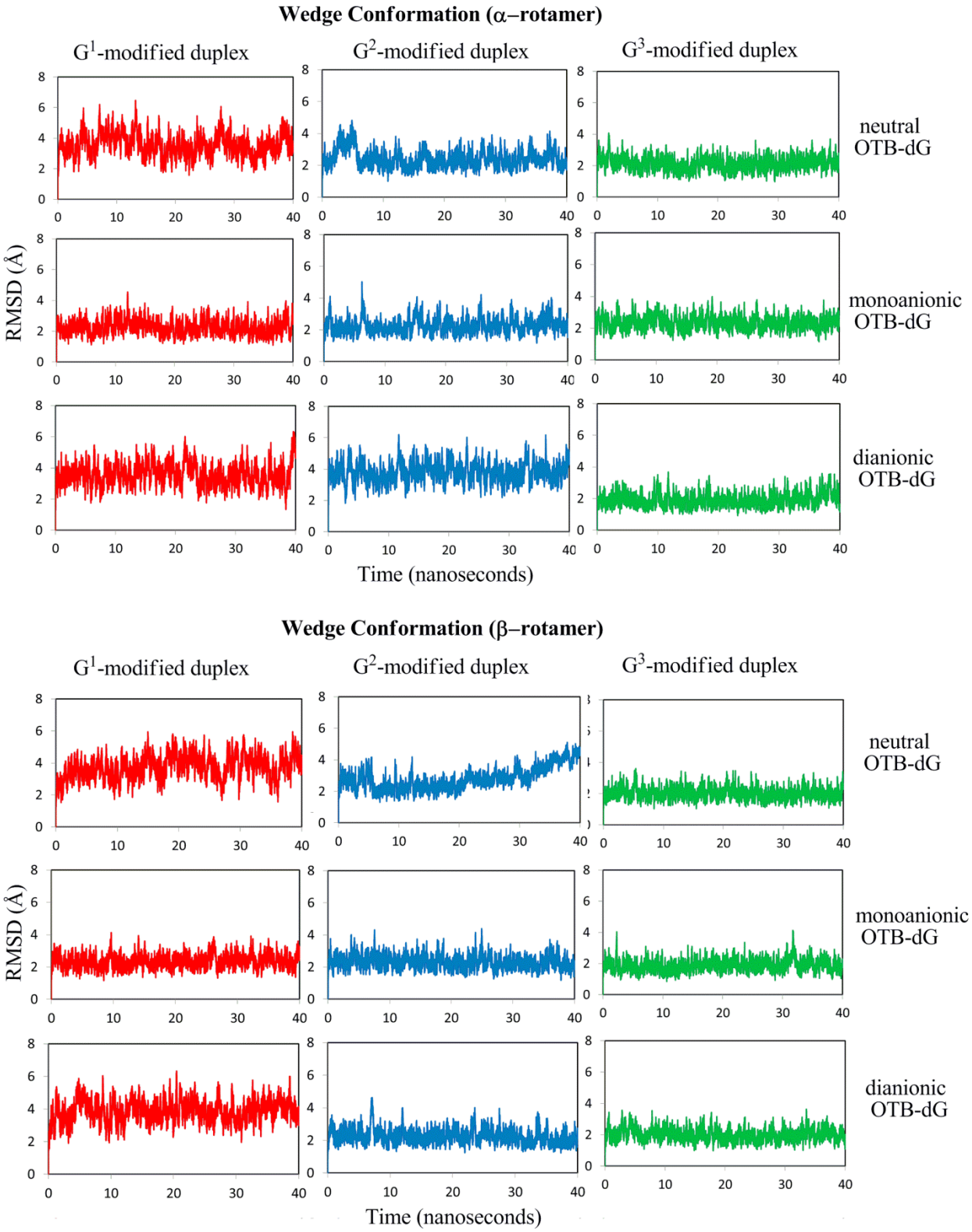

Figure S9. Backbone RMSD versus time for the wedge conformations of the OTB-dG adducted DNA with the adduct in three positions and ionization states.

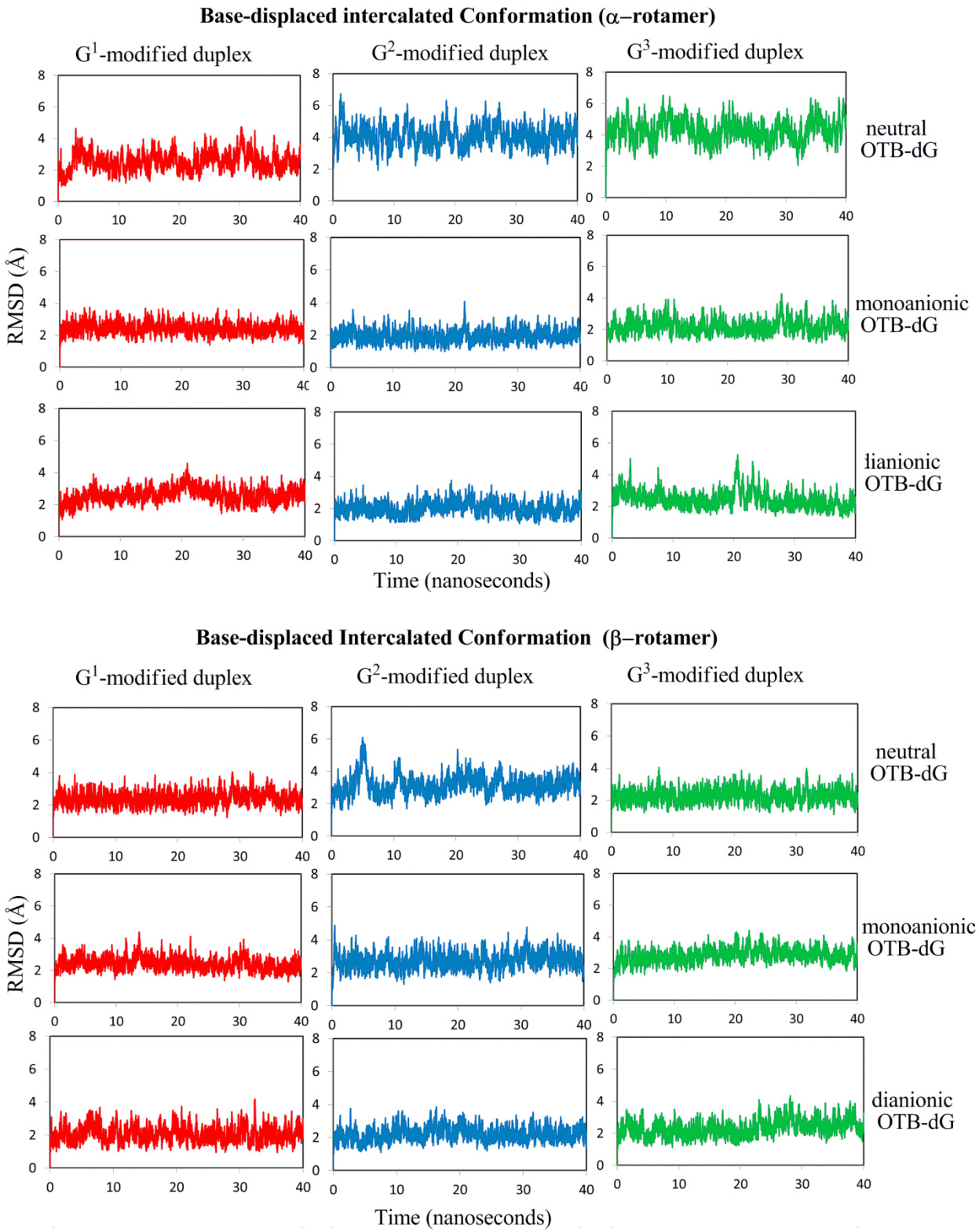

Figure S10. Backbone RMSD versus time for the base displaced intercalated conformations of the OTB-dG adducted DNA with the adduct in three positions and ionization states.

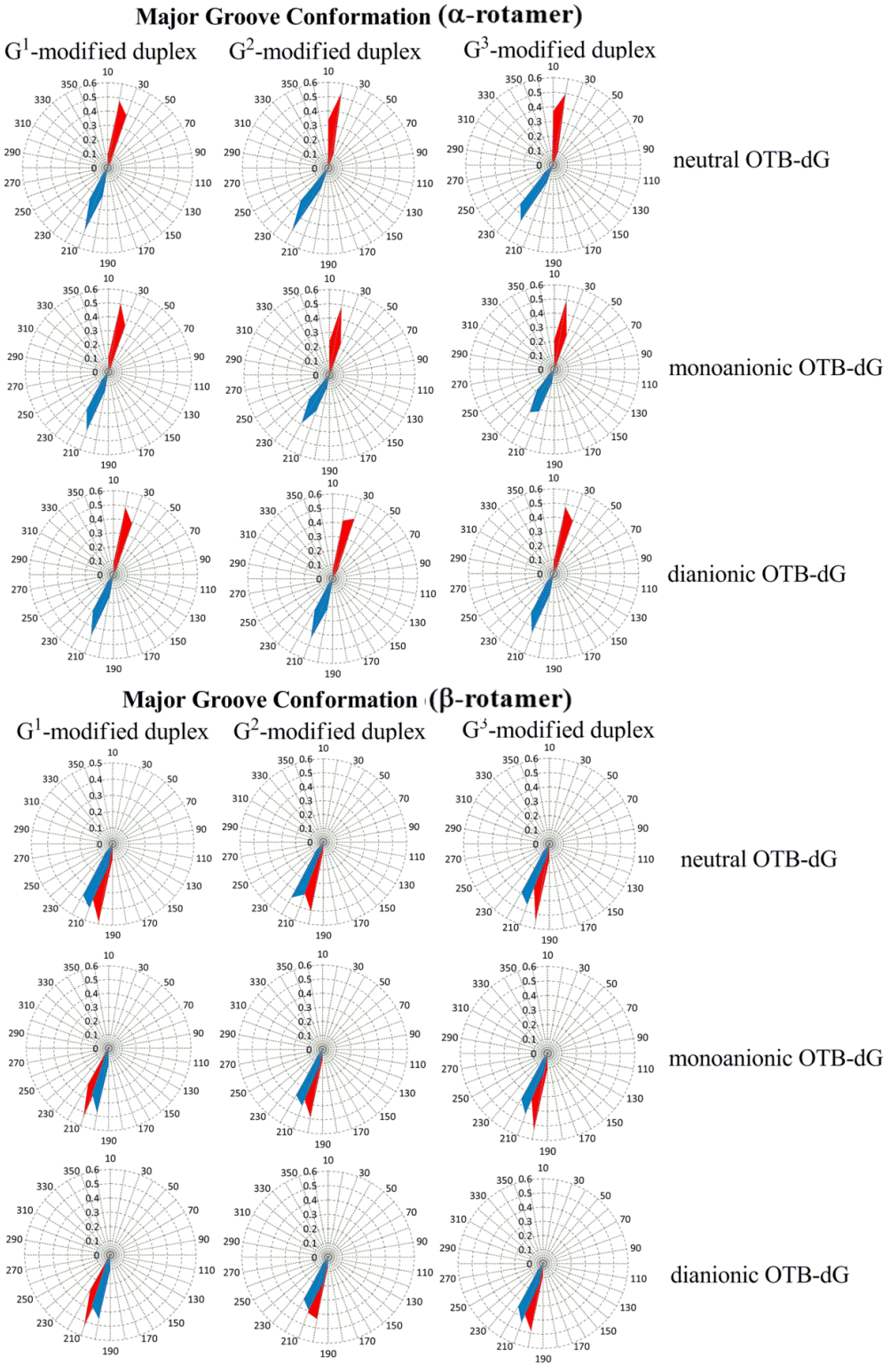

Figure S11. Radar plots for the probability distribution of the χ (blue) and θ (red) torsion angles for the major-groove conformations of OTB-dG adducted DNA with the lesion in two rotamers, three positions and three ionization states.

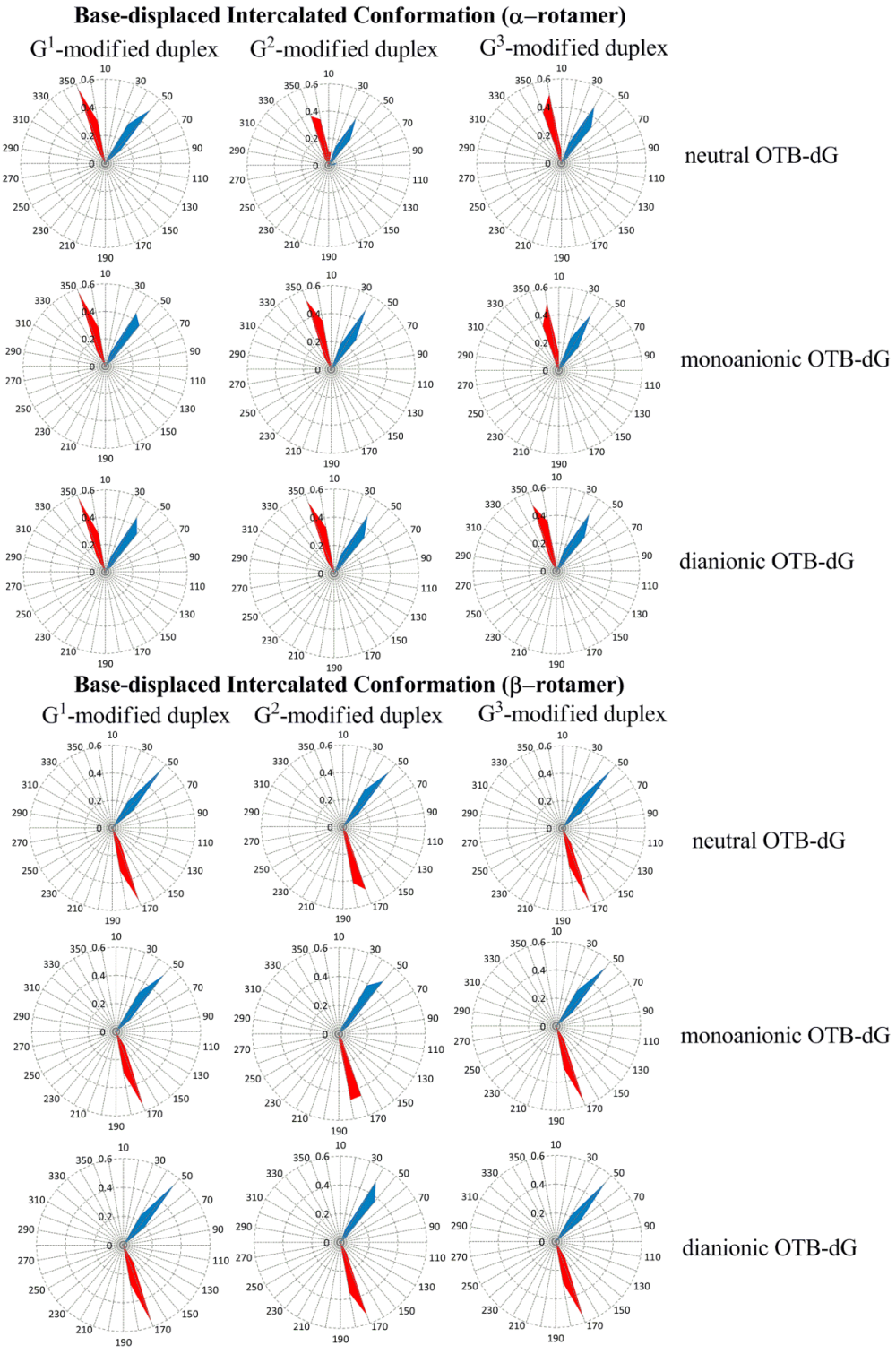

Figure S12. Radar plots for the probability distribution of the χ (blue) and θ (red) torsion angles for the base-displaced intercalated conformations of OTB-dG adducted DNA with the lesion in two rotamers, three positions and three ionization states.

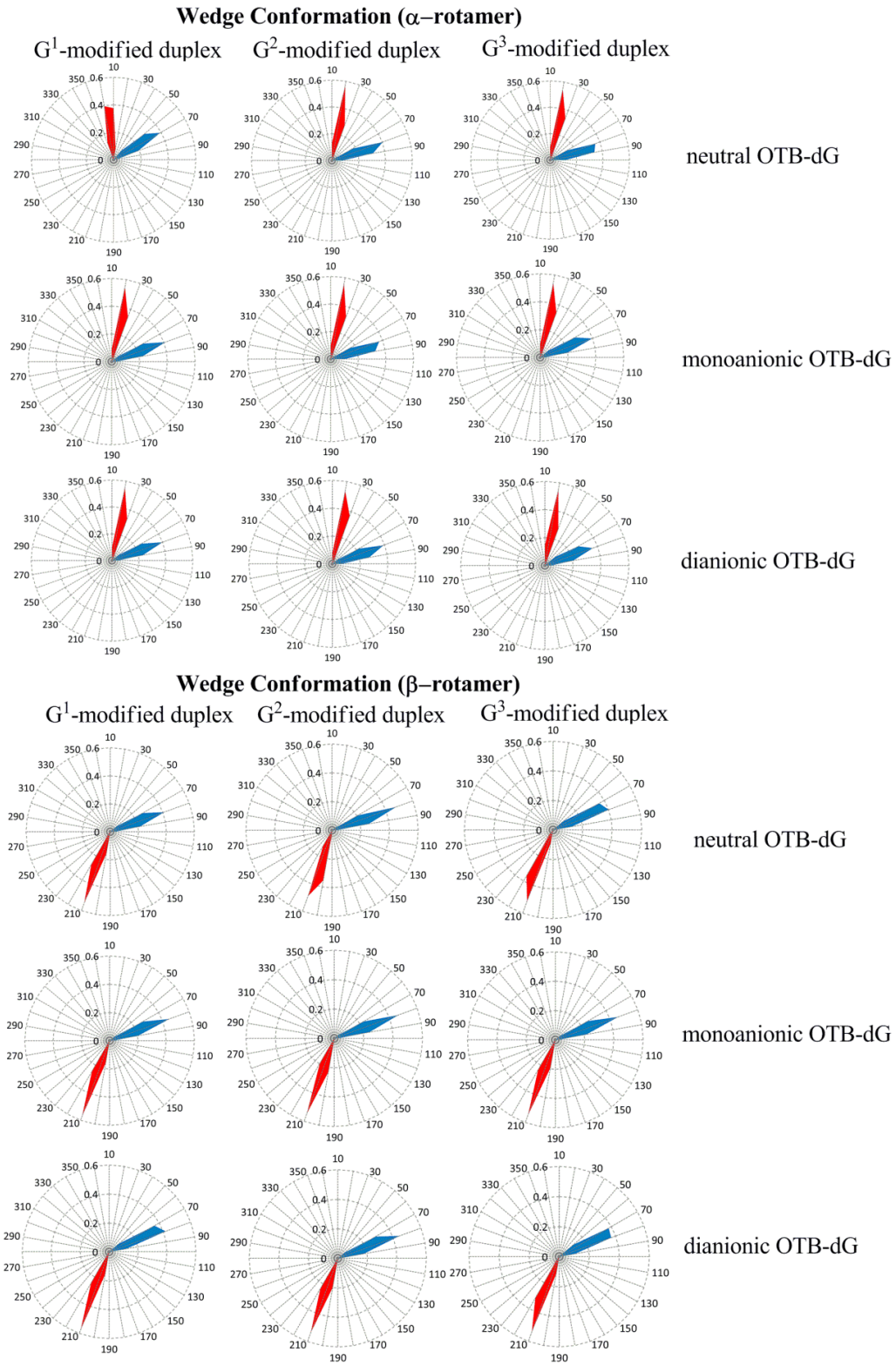

Figure S13. Radar plots for the probability distribution of the χ (blue) and θ (red) torsion angles for the wedge conformations of OTB-dG adducted DNA with the lesion in two rotamers, three positions and three ionization states.

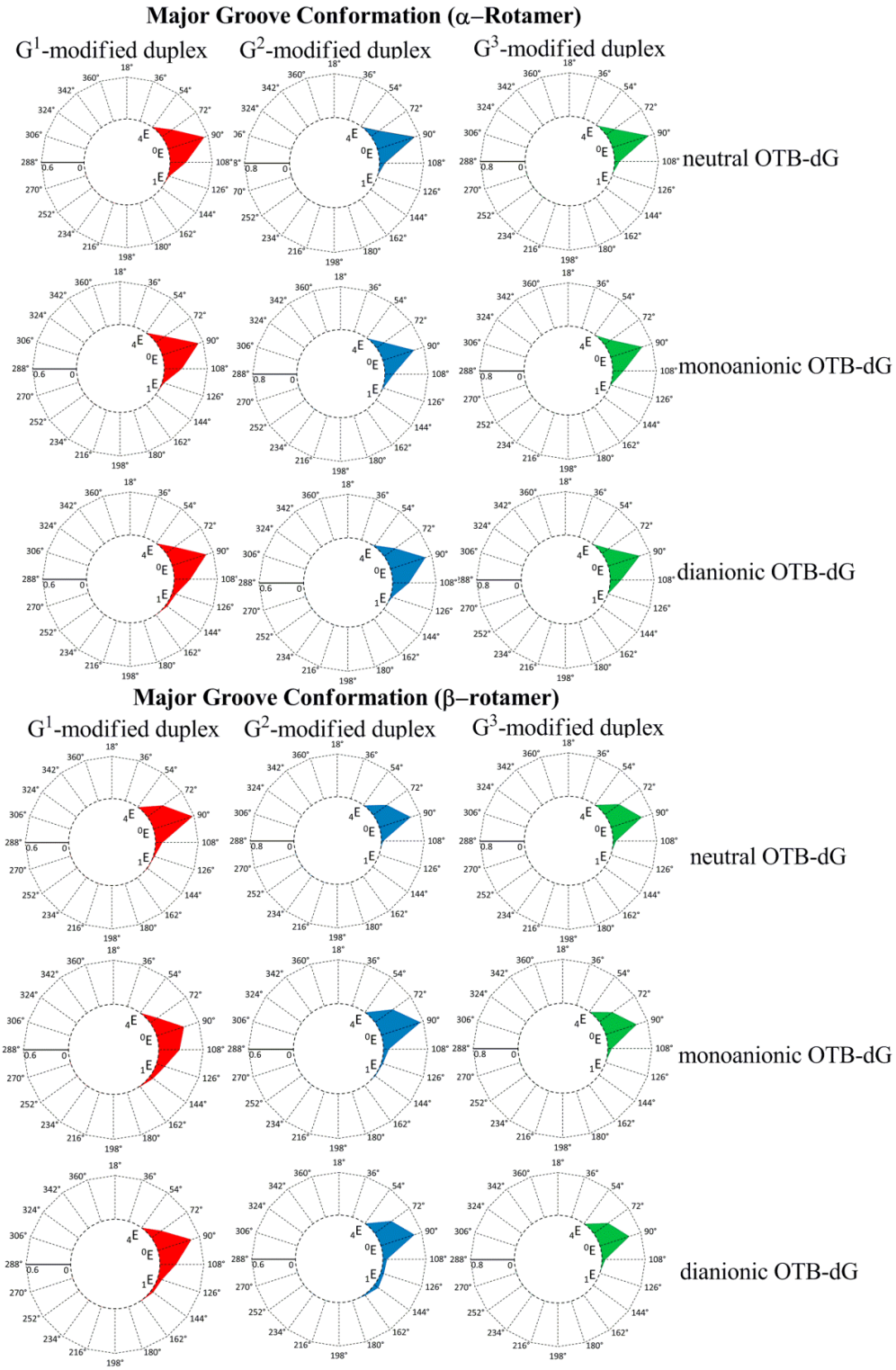

Figure S14. Pseudorotation plots showing the probability distribution of the sugar pucker for the major groove conformations of OTB-dG adducted DNA with the lesion in two rotamers, three positions and three ionization states.

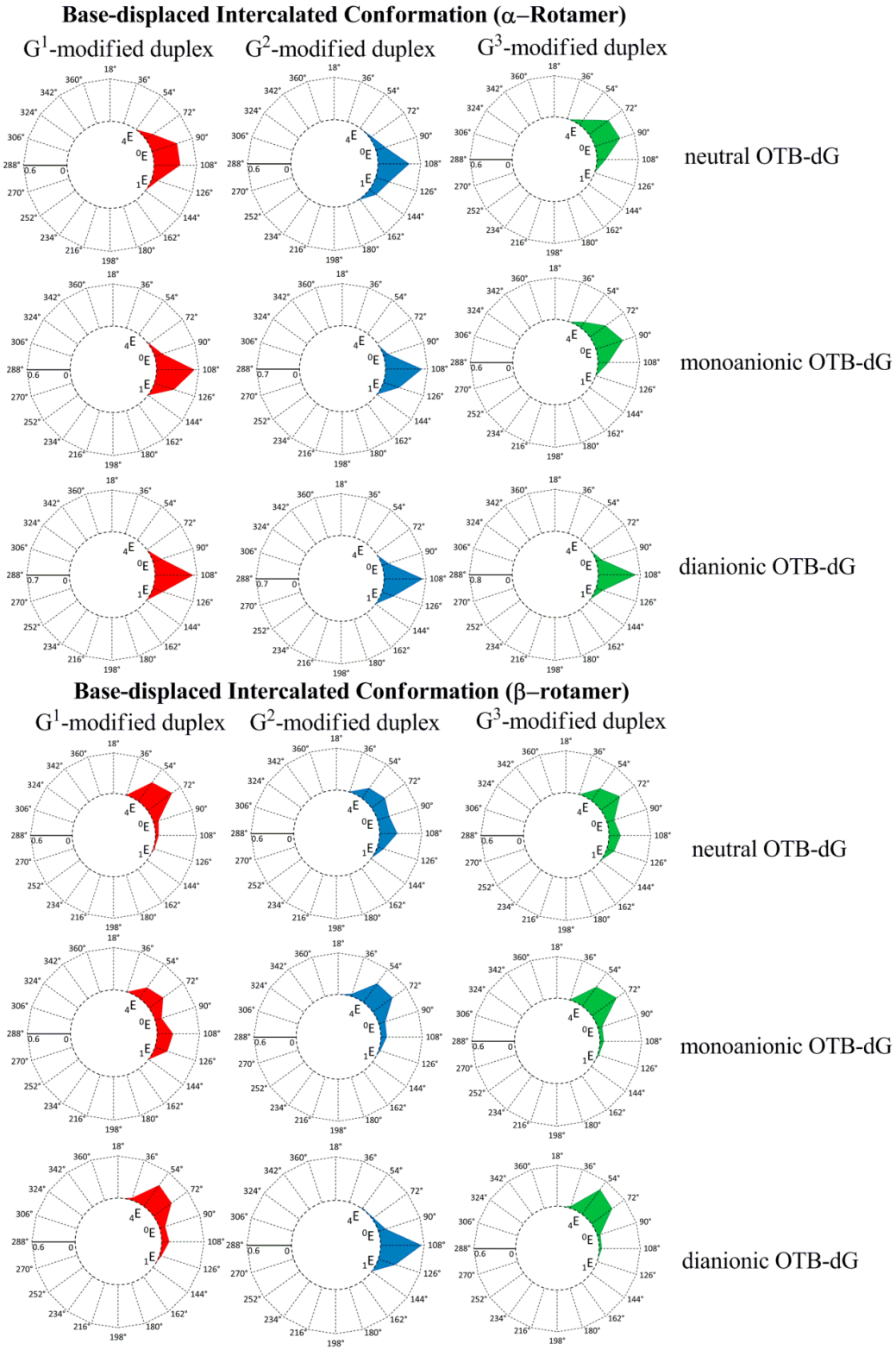

Figure S15. Pseudorotation plots showing the probability distribution of the sugar pucker for the base-displaced intercalated conformations of OTB-dG adducted DNA with the lesion in two rotamers, three positions and three ionization states.

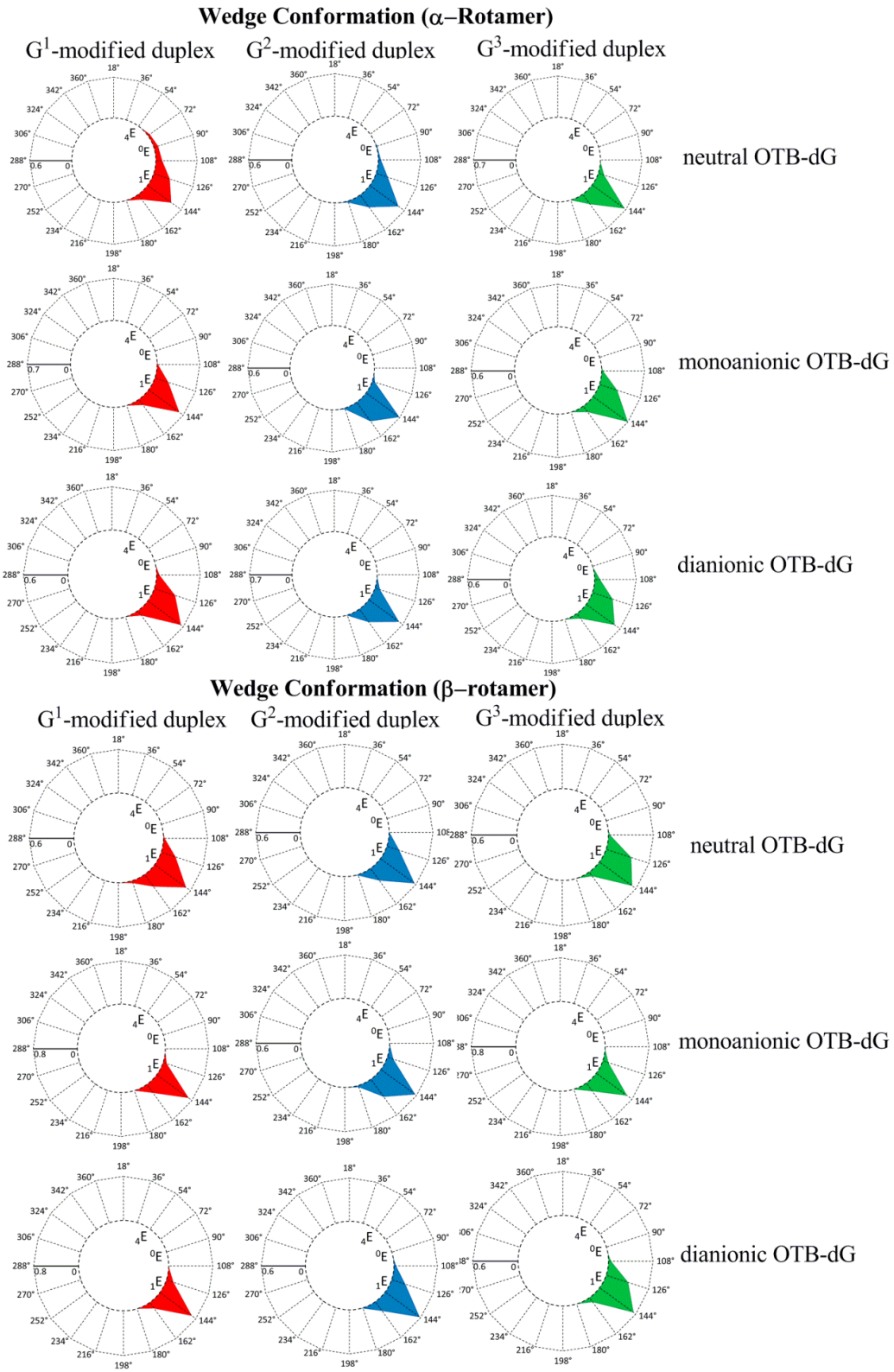

Figure S16. Pseudorotation plots showing the probability distribution of sugar pucker for the wedge conformations of OTB-dG adducted DNA with the lesion in two rotamers, three positions and three ionization states.

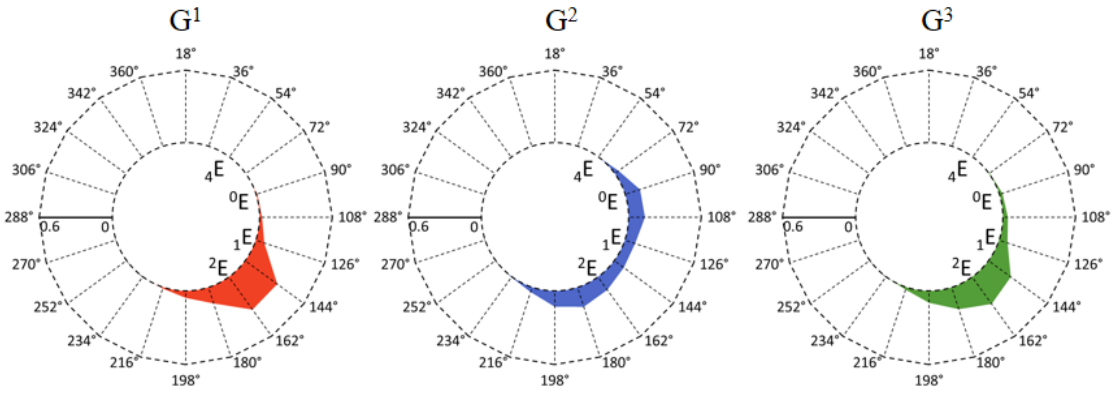

Figure S17. Pseudorotation plots showing the probability distribution of the sugar pucker at the G^1, G^2 and G^3 positions in the natural *Nar*I helix.

References

1. Case, D.A., Darden, T.A., T.E. Cheatham, I., Simmerling, C.L., Wang, J., Duke, R.E., Luo, R., Crowley, M., R.C.Walker, Zhang, W., Merz, K.M., B.Wang, Hayik, S., Roitberg, A., Seabra, G., Kolossváry, I., K.F.Wong, Paesani, F., Vanicek, J., Wu, X., Brozell, S.R., Steinbrecher, T., Gohlke, H., Yang, L., Tan, C., Mongan, J., Hornak, V., Cui, G., Mathews, D.H., Seetin, M.G., Sagui, C., Babin, V. and Kollman, P.A., *Amber 11*. 2010, University of California, San Francisco, CA.
2. Wang, J., Wolf, R.M., Caldwell, J.W., Kollman, P.A. and Case, D.A. (2004) Development and testing of a general AMBER force field. *J. Comput. Chem.* **25**, 1157–1174.
3. Dupradeau, F.-Y., Pigache, A., Zaffran, T., Savineau, C., Lelong, R., Grivel, N., Lelong, D., Rosanski, W. and Cieplak, P. (2010) The R.E.D. Tools: Advances in RESP and ESP charge derivation and force field library building. *Phys. Chem. Chem. Phys.* **12**, 7821-7839.
4. Sharma, P., Manderville, R.A. and Wetmore, S.D. (2013) Modeling the conformational preference of the carbon-bonded covalent adduct formed upon exposure of 2′-deoxyguanosine to ochratoxin a. *Chem. Res. Toxicol.* **26**, 803-816.
5. Wang, J., Wang, W., Kollman, P.A. and Case, D.A. (2006) Automatic atom type and bond type perception in molecular mechanical calculations. *J. Mol. Graph. Model.* **25**, 247–260.
6. Case, D.A., Darden, T.A., T.E. Cheatham, I., Simmerling, C.L., Wang, J., Duke, R.E., Luo, R., Walker, R.C., Zhang, W., Merz, K.M., Roberts, B., Hayik, S., Roitberg, A., Seabra, G., Swails, J., Goetz, A.W., Kolossváry, I., Wong, K.F., Paesani, F., Vanicek, J., Wolf, R.M., Liu, J., Wu, X., Brozell, S.R., Steinbrecher, T., Gohlke, H., Cai, Q., Ye, X., Wang, J., Hsieh, M.-J., Cui, G., Roe, D.R., Mathews, D.H., Seetin, M.G., Salomon-Ferrer, R., Sagui, C., Babin, V., Luchko, T., Gusarov, S., Kovalenko, A. and Kollman, P.A., *Amber 12*. 2012, University of California, San Francisco, CA.
7. Jorgensen, W.L., Chandrasekhar, J., Madura, J.D., Impey, R.W. and Klein, M.L. (1983) Comparison of simple potential functions for simulating liquid water. *J. Chem. Phys.* **79**, 926–935.
8. Miller, B.R., McGee, T.D., Swails, J.M., Homeyer, N., Gohlke, H. and Roitberg, A.E. (2012) MMPBSA.Py: An efficient program for end-state free energy calculations. *J. Chem. Theory Comput.* **8**, 3314–3321.